Author/s:
Graham, KL;McCowan, CI;Caruso, K;Billson, FM;Whittaker, CJG;White, A

Title:
Optical coherence tomography of the retina, nerve fiber layer, and optic nerve head in dogs with glaucoma

Date:
2020-01-01

Citation:
Graham, K. L., McCowan, C. I., Caruso, K., Billson, F. M., Whittaker, C. J. G. & White, A. (2020). Optical coherence tomography of the retina, nerve fiber layer, and optic nerve head in dogs with glaucoma. Veterinary Ophthalmology, 23 (1), pp.97-112. https://doi.org/10.1111/vop.12694.

Persistent Link:
https://hdl.handle.net/11343/286145

DR KATHLEEN LOUISE GRAHAM (Orcid ID : 0000-0003-2548-2969)

Article type : Original Report

Optical coherence tomography of the retina, nerve fiber layer and optic nerve head in dogs with glaucoma

Kathleen L. Graham[a] BVSc(Hons1) MVS MANZCVS

Christina I McCowan[b,c] BVSc BSc(Hons) PhD MANZCVSc DACVP

Kelly Caruso[d] BSc VMD DACVO

F. Mark Billson[e] BVSc PhD DVOphthal DipVetClinStud MANZCVS

Cameron J.G. Whittaker[d] BVSc DVCS MACVSc DACVO

Andrew White[a,f] BMedSci(Hons) MBBS PhD FRANZCO

[a] Clinical Ophthalmology and Eye Health, Sydney Medical School, University of Sydney, NSW Australia

[b] University of Melbourne Veterinary Hospital, University of Melbourne; Victoria Australia

[c] Department of Economic Development, Jobs, Transport and Resources, Victoria Australia 3000

[d] Eye Clinic for Animals, Crows Nest, NSW Australia 2065

[e]Small Animal Specialist Hospital, North Ryde, NSW Australia 2113

[a,f]Westmead Institute for Medical Research, Westmead, NSW Australia 2145

Corresponding author: Kathleen Graham

Email: kathleen.graham@sydney.edu.au

Keywords: canine, glaucoma, OCT, optic nerve head, retina, RNFL

Running title: Retinal thickness in dogs with glaucoma

Abstract

Objective To evaluate the retina and optic nerve head (ONH) in canine eyes predisposed to glaucoma using optical coherence tomography (OCT).

Animals Twenty-five eyes (24 dogs)

Methods Measures of peripapillary retinal, retinal nerve fiber layer (RNFL), and ganglion cell complex (GCC) thickness and ONH parameters were obtained *in vivo* by OCT of the unaffected eye in dogs diagnosed with unilateral primary glaucoma (*predisposed*; n=12) and compared with measures of healthy control eyes (*normal*; n=13). Repeatability and intra-rater reliability were explored using intraclass correlation coefficients (ICC).

Results Compared to normal eyes, predisposed eyes had a thinner retina in the temporal (p=0.005) and inferior quadrants (p=0.003) and decreased inner retinal thickness (superior: p=0.003, temporal: p=0.001, inferior: p<0.001, nasal: p=0.001). Predisposed eyes had a thinner RNFL compared to normal eyes (p=0.005), and when analyzed in quadrants, was thinner in the superior (p<0.001), temporal (p=0.034), and nasal quadrants (p=0.001). Repeatability (ICC 0.763-0.835) and intra-rater reliability (ICC 0.824-0.942) were good to excellent for measures of retinal thickness, and adequate for RNFL measurements (ICC 0.701-0.798). Reliable measurements of optic disc area were obtained and were similar between groups (p=0.597). Measurements of

parameters relying on automated software detection (GCC, optic cup, optic rim) had inadequate repeatability and reliability.

Conclusion Statistically significant differences in retinal and RNFL thicknesses were identified in normal and predisposed eyes. Reliable and consistent measurements of variables with manual adjustment of software detected parameters were obtained. Validation of OCT as a diagnostic tool for clinical assessment in canine glaucoma is warranted.

Introduction

Glaucoma is a neurodegenerative disease that results in structural changes to the retina and optic nerve head (ONH) and associated progressive vision loss. These structural and functional changes occur due to retinal ganglion cell (RGC) and axonal loss, although the exact nature of the structure-function relationship in glaucoma remains unknown.[1] Experimental and clinical investigations in people with primary open angle glaucoma (POAG) vary with respect to which changes occur first, whether structure and function are indeed correlated, and how these correlations change with disease progression.[2-8] Possible reasons for inconsistencies between studies in people include differences in study populations, the presence and type of glaucoma, stage of disease, and the sensitivity and specificity of tests and parameters used to detect change.[1,8]

Pattern-evoked ERG and automated perimetry provide objective measures of inner retinal and visual function that are not widely available or not practical in veterinary medicine, and despite reports describing tools to measure canine visual function,[9-16] vision is difficult to quantify in dogs and visual field deficits are rarely detected in this species. The identification of ONH damage in dogs is complicated by the degree of variation in ONH appearance with myelin extending anterior to the lamina cribrosa in this species.[17] Despite the inadequacy of intraocular pressure (IOP) alone for the identification of glaucoma and its progression,[18,19] the diagnosis and monitoring of canine glaucoma is primarily based on an elevated IOP and/or clinical features indicative of chronic

IOP elevation, and availability of technologies that can identify early structural changes in the posterior segment is limited in veterinary practice.

Identification of structural changes before the onset of clinically recognizable disease could facilitate diagnosis of glaucoma at earlier stages than is currently possible. Optical coherence tomography (OCT) is a high-resolution optically based imaging system that uses low-coherence interferometry to provide cross-sectional images of ocular tissues.[20] The use of OCT to evaluate the ONH, retinal nerve fiber layer (RNFL), and the macula is common in people with glaucoma,[2-4,21,22] and new approaches in the use of OCT in glaucoma management continue to emerge.[23-26] Despite widespread use of OCT in clinical ophthalmic and optometry settings for people, the use of OCT for assessment of the canine posterior segment remains limited, although its use has been increasingly reported over the last decade. Veterinary use of OCT for assessment of the posterior segment is reported in normal Beagles,[27,28] dogs with Sudden Acquired Retinal Degeneration Syndrome (SARDS),[29-31] in research settings investigating diseased retinas,[32-36] in cats,[37,38] and in case reports describing a variety of retinal conditions.[39-42] Grozdanic et al[43] reported thinning of the inferior retina as measured by OCT following induction of an acute elevation in IOP in normal Beagles. However, to the authors' knowledge, there are no published reports of systematic studies of these OCT parameters in eyes with glaucoma or eyes at risk of glaucoma in dogs.

In this cross-sectional study, we evaluated the ability of spectral-domain OCT (SD-OCT) to detect structural changes consistent with disease in the predisposed fellow eye of dogs with naturally occurring glaucoma.

Materials and Methods

Animals

Privately owned pet dogs with unilateral primary angle closure glaucoma, as diagnosed by a veterinary ophthalmologist, and healthy control dogs without ophthalmic disease, were included. All dogs had a complete physical and ophthalmic examination, including slit lamp biomicroscopy (Keeler PSL Classic Portable Slit Lamp, Keeler Ltd, UK), indirect ophthalmoscopy (Welch Allyn Australia Pty Ltd, NSW Australia), quantitative tear testing (Schirmer tear test, Merck Animal Health, NJ, USA), rebound tonometry (Icare® Tonovet, Icare, Finland) and fluorescein staining. Gonioscopy was performed using a direct (Koeppe, Ocular Instruments, Bellevue, WA, USA) or indirect (G-4 Four Mirror, Volk Optical Inc, Mentor, OH, USA) goniolens according to clinician preference, and findings recorded as either normal or abnormal. Ultrasound biomicroscopy (UBM; 48MHz probe, Accutome, UBM Plus 24-6300-G-V, Malvern PA) of the anterior segment was performed on every eye that was included in analyses, and B-mode ultrasonography (10MHz probe, Philips HD-11, Philips Australia) performed in all dogs with glaucoma to support the absence of any intraocular structural change that may result in secondary glaucoma. All procedures were conducted with approval from the University of Sydney Animal Ethics Committee (2016/1004), and with the informed consent from the dog's owner.

Eyes were allocated into groups based on the following criteria: (i) *normal*: eyes with an unremarkable ophthalmic examination, no abnormalities on gonioscopy, and no clinical or historical suggestion of vision impairment; (ii) *predisposed*: eyes with an abnormal drainage angle on gonioscopy (narrowed iridocorneal angle and/or pectinate ligament dysplasia), a narrowed or collapsed ciliary cleft on UBM examination, and a diagnosis of primary angle closure glaucoma (PACG, clinical diagnosis with or without supportive histopathologic changes) in the contralateral eye made by a veterinary ophthalmologist. Measures of retinal thickness and the ONH were compared between normal eyes and those predisposed to glaucoma. Medical records were reviewed, and clinical data including signalment, histopathology of previously enucleated globes (where available), IOP and duration of clinical signs recorded.

Procedures

Image acquisition was performed after physical and ophthalmic examinations. Rebound tonometry was repeated after application of one drop of tropicamide 1.0% (Minims, iNova Pharmaceuticals Pty Ltd, Chatswood, NSW Australia) had resulted in pupil dilation, and before administration of any sedative. The cornea was lubricated throughout imaging procedures with 0.3% hypromellose (GenTeal Eye Gel, Alcon Laboratories Australia Pty Ltd, Frenchs Forest NSW). Imaging was performed under sedation except if the dog was anaesthetized for reasons separate to this study in which case images were obtained at the beginning of the anesthetic. Sedation typically included medetomidine (2-5µg/kg IV, Domitor, Pfizer Ltd. West Ryde, NSW) and butorphanol (0.1-0.2mg/kg IV,

Torbugesic, Zoetis Australia Pty Ltd. Rhodes NSW Australia) administered to effect. After all scans were obtained, sedation was reversed using atipamezole (Antisedan, Pfizer Ltd. West Ryde, NSW).

Image acquisition

All images were obtained using the Optovue iVue SD-OCT unit (Optovue, Inc., Freemont, CA USA) with an image acquisition rate of 25,000 axial scans (A-scans) per second with 5μm depth resolution. Imaging of all eyes was performed by the same investigator and this investigator stabilized the globe and operated the OCT unit. Following pupil dilation, oxybuprocaine hydrochloride 0.4% (Minims, iNova Pharmaceuticals Pty Ltd, Chatswood NSW Australia) was administered topically and Colibri forceps used to hold the conjunctiva near the limbus at 12 o'clock for manipulation and stabilization of the globe. The OCT device was mounted on a tripod with a ball head mount and the height and angle adjusted for imaging of each eye. Scanning was centered over the ONH to capture all sectors of the peripapillary retina (Fig.1).

Quality of the scanned image, calculated by the manufacturer's software as the scan quality index (SQI), was affected by the intensity of reflected light. Data for analyses were obtained from a scan with 'good' SQI for each structure investigated (retinal thickness, RNFL, GCC, ONH). Greater light intensities resulted in a higher SQI. These SQI data were classified as 'good' or 'poor' by the software. Scans classified as 'poor' did not allow ocular structures/layers to be visible and easily segmented and were repeated until a scan with a 'good' SQI

was obtained for analysis. When the signal strength was 'poor' due to pathology or miosis affecting light absorption, that eye was excluded from the study.

Other factors that resulted in poor images that could not be used included a local weak signal, data that were out of the OCT window boundary, and poor positioning. Weak signals (caused by blinking, poor alignment etc.) resulted in an inability to visualize retinal layers on the image (B-scan). When data were either too high or too low in the OCT window boundary, accurate data acquisition was compromised and affected scans were discarded (Fig.2a). Globe position was assessed by evaluating the position of the dorsal retinal vein on en face images, and by assessing horizontal and vertical retinal scans (retina cross line scan). If the dorsal retinal vein, including the detectable thickness associated with that vessel, remained in the superior quadrant, the image was considered satisfactory (Fig.2b). If the globe was rotated such that the dorsal retinal vein and its associated retinal thickness was outside the superior quadrant, the scan was discarded (Fig.2c). Scans where the retina was tilted in one or both of the horizontal and/or vertical plane (Fig.2d), were either repeated so that the retina was flat (Fig.2e), or the eye was excluded from the study. In scans of the ONH (and, consequently, corresponding RNFL measurements), scan quality was affected if not centered on the optic disc, and where the scan was not centered on the ONH, the case was excluded from ONH analyses.

Scan adjustments and segmentation

For each eye, the series of scans obtained included: retinal scans (retinal map and crossline), ONH and RNFL assessment (one 3D glaucoma scan to obtain the

baseline optic disc for manual adjustment of the optic disc outline, and a subsequent glaucoma scan for measurement of the optic disc and nerve fiber layer parameters), and one scan for ganglion cell complex analysis.

To determine retinal thickness, retinal scans centered on the ONH, were obtained for each eye, and thickness of the peripapillary retina recorded for analyses based on a single scan for each subject (Fig.3). Total retinal thickness was measured from the inner limiting membrane (ILM) to the retinal pigment epithelium (RPE), inner retinal thickness from ILM to the outer limit of the inner plexiform layer (IPL), and the outer retina from the IPL to the RPE (Fig.4). Manual adjustments of software-derived measurements were made to each of the 20 composite B-scan images obtained in each retinal scan. To eliminate the influence of ONH myelination, lines demarcating the boundaries measured (ILM, IPL, and RPE), were manually adjusted to overlay each other over the region of the ONH and myelin (between the ends of the RPE) (Fig.5).

For calculation of RNFL thickness and ONH parameters, glaucoma scans (3D and standard scans) were centered on the ONH and included a circle with diameter 3.45mm. Each scan pattern consisting of 13 concentric circular scans ranging from 1.3 to 4.9mm diameter with 0.3mm interval, and 12 radial scans 3.4mm in length was used in analysis of the ONH. Automated detection of the optic disc margin, as well as the ends of the RPE/choroid complex, which were adjusted on the 3D ONH images, were manually corrected prior to analysis (Fig.6). No manual corrections were made (not possible with the instrument's proprietary software) to detection or measurement of the optic cup or rim in any study.

The GCC consisted of those retinal layers in which retinal ganglion cells were located. This included the RNFL containing ganglion cell axons, the ganglion cell layer containing ganglion cell bodies, and the IPL containing the ganglion cell dendrites. The scan protocol used to obtain measures of GCC consisted of 15,000 points in a 7mm square area within 0.6sec using one horizontal line and 15 vertical lines at 0.5mm intervals. GCC scans were centered 0.75mm temporal to the ONH. Detection and measurement of the GCC was automated for all studies with no manual adjustments possible using the instrument's proprietary algorithm for this setting. GCC scans were excluded only if not appropriately centered temporal to the ONH.

Repeatability of scanning technique

To evaluate the consistency of measures obtained between scans of the same dog under the same conditions, the entire series of scans were obtained twice (under the same sedation) in 11 dogs (11 eyes). Intra-class correlation coefficient (ICC) was calculated for each variable obtained in sequential scans of the same eye.

Reliability of observer measurements

To evaluate intra-rater reliability in making manual adjustments to the segmentation of retinal layers and ONH, the same observer performed manual adjustments and obtained a repeat series of measurements for each eye to obtain a new dataset for comparison to the initial measurements obtained, with a 6 month period between analyses to avoid any risk of recall bias. Reliability of the

GCC analyses was not assessed as these variables were automated measures that could not be manually adjusted.

Statistical Analyses

Data were analyzed using commercially available software (SPSS v22.0, IBM Corporation; GraphPad Prism 7.0a). Individual characteristics of dogs/eyes in each group were compared using a Mann-Whitney test for continuous variables (age, IOP, duration of disease), and a Fisher exact test was used to compare categorical data between study groups (pure- versus crossbred, sex, eye). A Mann-Whitney test was used to compare measurements of each variable between normal and predisposed eyes.

Spearman's rank-order correlation was used to determine the strength and direction of association of age, IOP, and the duration of glaucoma (when relevant) with measured variables. Regional differences (between peripapillary quadrants) in retinal thickness between eyes in the same group were compared using a Kruskal-Wallis non parametric ANOVA and Dunns multiple comparisons test. The effect of group (ophthalmic diagnosis) on dependent variables was assessed using a Mann-Whitney test as non-parametric data did not satisfy assumptions of a t-test. When two eyes from the same dog were included in the study, the mean of both eyes for each variable was used for analyses. For all analyses, a p value <0.05 was considered statistically significant.

In assessing repeatability and intra-observer reliability with the ICC, a one-way random model was assumed where the subjects (dogs) are assumed random.[44]

Correlations >0.9 were considered excellent, when 0.80-0.89 they were considered good, when 0.70-0.79 correlations were considered adequate, and correlations <0.70 were considered of limited applicability.[45]

Results

Images suitable for analyses were obtained of 25 eyes from 24 dogs to assess for potential changes in the retina and ONH of eyes predisposed to glaucoma (Table 1). Twelve dogs (13 eyes) were normal, and 12 dogs (12 eyes) predisposed to primary glaucoma. Of the 12 predisposed dogs, the contralateral glaucomatous eye was still present in seven cases. Scanning of eyes with glaucoma was precluded by prostaglandin analogue-induced miosis in five cases. The remaining two glaucomatous eyes (cases 13 and 20) were diagnosed with PACG on the day of scanning. For ethical reasons, treatment with IOP lowering medication (topical latanoprost) was not delayed for imaging. The initial scans for both eyes were unsuitable for analysis, and the development of miosis with lowering of IOP precluded repeat scanning. Scans of six normal eyes were also excluded due to angulation of the scans (n=5) and globe rotation (n=1).

There was no statistically significant difference in age (p=0.231), sex (p=0.400), IOP (p=0.366) and the number of purebred dogs (p=1.000) between groups (Table 2). Following pharmacologic pupil dilation, the median IOP in eyes predisposed to glaucoma (17mmHg [interquartile range [IQR = 15-19mmHg]) was significantly higher than that in normal eyes (12.5mmHg [IQR 12-15.5mmHg]) (p=0.023).

There was no statistically significant correlation between age and any measure of retinal thickness or ONH parameter in either normal or predisposed eyes. No correlation was identified between any variable measured in predisposed eyes and the duration of glaucoma in that dog (time since diagnosis of glaucoma in the contralateral eye). In eyes predisposed to glaucoma, a moderate positive correlation was identified between the IOP following pharmacologic pupil dilation and RNFL thickness in the superior (r=0.782, p=0.010), and in the inferior retina (r=0.702, p=0.028).

Retinal thickness

Table 3 presents median retinal thickness in each peripapillary region assessed. In normal eyes, total retinal thickness in the superior quadrant was significantly thicker than in both the inferior (p=0.010) and nasal quadrants (p=0.025). The inner retina was significantly thicker in the superior compared to the inferior quadrant (p=0.021), but no statistically significant difference was identified in outer retinal thickness between peripapillary quadrants (p=0.120) in normal eyes. When comparing regional differences in predisposed eyes, both total and outer retinal thickness values in the superior quadrant were significantly greater than in the temporal (p=0.016 and 0.012, respectively) and inferior quadrants (p=0.008 and 0.023, respectively), and inner retinal thickness significantly greater in the superior quadrant compared to the inferior quadrant (p=0.020).

In predisposed eyes, median total retinal thickness was significantly thinner in the temporal (162µm, 95% CI [134, 173]) and inferior quadrants (158µm, 95%

CI [137, 169]) compared to normal eyes (temporal: 186μm 95% CI [175, 202]; inferior: 178μm, 95% CI [172, 187]) (p=0.005 and 0.003 respectively) (Fig.7). The inner retina was significantly thinner in predisposed eyes in all quadrants compared to inner retinal thickness in normal eyes (Fig.8). There was a statistically significant difference in outer retinal thickness between groups only in the superior quadrant, where the outer retina in predisposed eyes (116μm, 95% CI [102, 121]) was thicker compared to that in normal eyes (101μm, 95% CI [91.5, 113]) (p=0.039).

Nerve fiber layer thickness

The median RNFL thickness for all regions assessed is presented in Table 4. There was no statistically significant difference in RNFL thickness between regions in either normal (p=0.054) or predisposed eyes (p=0.435).

Overall, the median peripapillary RNFL was significantly thinner in predisposed (62.5μm, 95% CI [48.7, 80.7]) compared to normal eyes (92.5μm, 95% CI [80, 109]) (p=0.005) (Fig.9). Predisposed eyes had a thinner RNFL that reached statistical significance in the temporal (normal: 82μm, 95% CI [64.4, 120]; predisposed: 51.5 μm, 95% CI [40.1, 78.1]), superior (normal: 105μm, 95% CI [96.5, 125]; predisposed: 80μm, 95% CI [59.7, 90.3]) and nasal quadrants (normal: 89.5μm, 95% CI [78.1, 110]; predisposed: 60.5μm, 95% CI [44.5, 72.3]) (Fig.10).

Optic nerve head analyses

The software failed to detect an optic cup in five eyes (normal n=2; predisposed n=3) (Fig.9a,c), meaning that only measures of disc area were obtained as part of the ONH analyses in these eyes. There was no statistically significant difference in any ONH parameter measured when comparing normal and predisposed eyes (Table 5).

Ganglion cell complex

Positioning for assessment of the GCC (scan centered temporal to the ONH) was acceptable in 12/13 normal eyes, and in 11/12 predisposed eyes. There was a tendency for a thinner GCC in predisposed compared to normal eyes, although the difference between groups did not achieve statistical significance (Table 6).

Repeatability of scanning technique

A second complete study that included all scans to assess the retina, RNFL, GCC and ONH was performed in 11 eyes (seven normal; four predisposed). For all measures of total, inner and outer retinal thickness, repeatability of measurements obtained from different scans was adequate (ICC 0.748-0.835) while all measures of the GCC were considered inadequate (ICC 0.488 – 0.604) (Table 7). In the ONH analysis, the optic disc area had good repeatability (ICC 0.873) (Fig.11), but the remaining ONH parameters were considered of limited applicability due to their relatively poor repeatability (ICC 0.592 – 0.689).

Reliability of observer measurements

Intra-rater reliability was determined for measures of retinal, RNFL thickness and ONH parameters. Intra-rater reliability was good or excellent (ICC>0.824)

for all measures of total, inner and outer retinal thickness, and adequate for measures of RNFL in all sectors (ICC 0.713-0.789) (Table 7). Intra-rater reliability of the optic disc area was considered excellent (ICC 0.942) (Fig.12), although when the optic cup to disc area and volume ratios were calculated based on automated optic cup volume detection, reliability of these ratios was only considered adequate (ICC 0.742 and 0.791 respectively).

Discussion

This study was designed to evaluate whether OCT-derived measures of the retina and ONH have potential to aid in the early clinical assessment of canine glaucoma. The ability to detect changes in eyes predisposed to glaucoma prior to the onset of overt clinical signs that indicate late stage, irreversible damage, may allow for timely initiation of therapy at a stage where treatment could be more efficacious than current methods allow. In this study we identified statistically significant differences in structural measures of the retina when comparing normal and predisposed eyes. Based on these findings, the authors suggest further investigation and validation of OCT as a diagnostic tool in canine glaucoma is warranted.

To the authors' knowledge, this is the first report that includes a heterogenous sample of dogs as the control population.[27-29,31,43] There are limitations in drawing direct comparisons between existing studies due to the different populations,[27-29,31,43] scanning protocols, OCT units,[27-29,31,43] and analyses.[27-29,31,43] A varying distribution of RGC density associated with nose length,[46] and

differences in the expression of the visual streak within and between breeds is reported in dogs.[47] Furthermore, in humans, SD-OCT measures of retinal and RNFL thickness, and ONH parameters are significantly correlated with age and race,[48-50] and myopia is shown to independently influence RNFL thickness. [51] It is therefore important to consider the populations being studied, their relevance to clinical disease in a heterogenous population, and the scant reports describing OCT findings in dogs, when evaluating results of this, and previous studies.

We identified a large degree of variability in measures of retinal thickness between sectors, and propose blood vessel orientation and ONH myelin as potential confounding effects. For practical reasons, we did not exclude every scan in which the dorsal retinal vein was not directed straight at the 12 o'clock position. A previous investigation into validity of RNFL measures using this device describe poorer reliability and repeatability of the measurements in sectors compared to quadrants.[27] We therefore believe considering measurements in quadrants (rather than sectors) more appropriate with this device and using this technique.

Despite the differences in populations and techniques, we identified similar general patterns to previous reports, with the inferior retina being thinner than the superior retina. Measures of average retinal thickness in our study fall within the range of what has previously been described in normal Beagles (inferior: 163.9[29] – 215.6µm[28,31]; superior: 198.2[29] – 218.1µm[28,31]). Using the definitions of inner and outer retinal thickness as recently reported (inner retina: inferior 92.0-105.0µm, superior 88.3-101.3µm; outer retina: inferior 99.6-107.8µm,

superior 113.6-116.4μm),[31] our results (inner retina: inferior 86μm, superior 107μm; outer retina: inferior 92μm, superior 101μm) show a similar pattern despite differences in technique, location and population.

Despite the major limitations outlined previously for measurements of RNFL thickness, repeatability between scans and reliability of measurements requiring limited manual adjustments (to the ONH outline and the termination of the RPE), were adequate. Use of this parameter may therefore provide information in clinical disease, even if the measurements obtained are not precise measures of the RNFL in isolation. Compared to the post-processing requirements for measures of retinal thickness (adjusting three lines on each of 20 composite images), RNFL measurements relied on automated software algorithms. The RNFL thickness scans may therefore be more readily accepted by clinicians for whom efficiency, and getting results at the time of testing would be of practical importance.

Variations in the location, depth, width and homogeneity of the peripapillary RNFL thickness using OCT occur in people,[52] and regional variation was recently described in a small number of healthy Beagles.[27,29] Median RNFL thicknesses in normal dogs in this series are similar to the manually adjusted mean values reported in those beagles,[27] but were greater than the RNFL thickness reported in the control group of dogs assessed in a study on SARDS using a different OCT unit.[29] The substantially thinner RNFL measures in control dogs in the latter study (superior-temporal RNFL thickness: 26.2±0.3μm; inferior-temporal: 24.9±0.4μm)[29] likely reflects significant differences in both hardware and

software algorithms used to establish these thickness values. Whereas regional differences in RNFL within an eye were described in beagles,[27] we did not identify regional differences in RNFL thickness in eyes within either group. This difference may be due to the small sample size in both study populations, the different populations studied (homogenous population of young healthy beagles compared to a heterogenous population of pet dogs), or due to the method of data analysis.

The identification of a thinner RNFL in predisposed compared to normal eyes, and the presence of a moderate correlation between RNFL thickness and the IOP following pharmacologic dilation in predisposed, but not in normal eyes is of particular interest. Neurodegeneration of RGCs is considered a hallmark of the diseases that comprise glaucoma, and in people with glaucoma, differing rates of structural change in the RNFL have also been reported between glaucoma progressors and non-progressors. [53-55] Further studies using OCT may provide additional evidence for how structural changes of the canine posterior segment *in vivo* might aid in diagnosis, prognostication and treatment of glaucoma in dogs.

A significant limitation of this study is that a single scan (for each structure) was used, with scanning and measurements performed by a single investigator. Our data therefore fail to account for subtle differences in measures related to differences in orientation. Good reliability and repeatability of measurements and scans were obtained for those variables that did not have automated measures (or parts thereof). For measures of RNFL thickness that are automated,

yet rely on manual adjustments of the ONH, both reliability and repeatability were considered adequate. When comparing the repeatability and intra-rater reliability achieved in this study with the single existing report describing inter- and intraobserver reliability in assessing RNFL thickness in normal beagles using the same OCT unit,[27] it is important to consider the differences in interpretation of the ICC between studies. We used the classic parameters for interpreting ICC[45], which are more conservative than those previously described.[27] Despite the limitations of having a single observer scan and measure all subjects in this study, from a practical standpoint, we demonstrate the technique as a tool that can be operated by a single person, which can have benefits in clinical practice. Establishing whether alternative techniques, for example having a separate person, or stay sutures to stabilize the globe, would improve repeatability of the scanning procedure, scan quality, or efficiency in the scanning procedure, is beyond the scope of this study.

Identification of the optic cup and disc in this series was not possible in all dogs and further investigation is paramount to determine the potential application and significance of these analyses. The only ONH parameter that could be accurately identified and manually delineated in this study was the optic disc area. The disc area measurements in our study were comparable to a previous report,[27] achieved good reliability and repeatability, and this parameter is therefore of potential clinical use. However, further studies, and possibly implementation of methods to manually identify, adjust and measure the optic cup and rim, are required before use of these automated measurements can be considered applicable or clinically relevant. Similar to measures of the optic cup

and rim, the GCC analysis relied on automated measurements and accurate positioning, with no ability to manually adjust the location or segmentation prior to analysis. This reliance on software, combined with limitations in accurately positioning the eye for follow up scans likely contributed to the poor repeatability and reliability in this study. Based on these findings, we suggest that the GCC analysis using the iVue proprietary software not be used for assessment of the retina without modification.

There is a considerable degree of overlap between groups in most parameters studied. This is not an unexpected finding with known differences in RGC density associated with breed and conformation,[46,47] variation in the presence and degree of intraocular myelin associated with the canine ONH, and our incomplete understanding of the pathophysiology of glaucoma. The extent of overlap in measurements between groups limits the use of a single OCT study as a stand-alone diagnostic test, but this is not unusual in veterinary diagnostics, and with validation, OCT may be a useful tool in the longitudinal clinical assessment of glaucoma in dogs, as applied in the management of glaucoma in people.

Limitations in what an OCT unit can achieve should be considered when evaluating studies, and potential uses of this technology in veterinary ophthalmology. The Optovue iVue unit used in this study was selected based on availability and cost, the fact it is portable and simple to use, and still provides the benefit of high scanning speeds associated with SD-OCT. The cost, and the

increasing availability of second hand units that may enter the veterinary market mean this type of device might be more accessible in veterinary clinical practice.

Some OCT units, such as the Heidelberg Spectralis (Heidelberg Industries), can detect and make adjustments so that the same area is imaged on serial scans. This feature is not available on the unit used in this study. A visible landmark was therefore imperative so serial measurements of the same structure and location can be made. The ONH has also previously been used as a landmark on which to center OCT studies because all nerve fiber bundles are directed toward it, and the peripapillary region is therefore indicative of changes throughout the retina despite regional variations.[27] However, the effect of retinal vasculature and intraocular myelin when using peripapillary measurements is more considerable, than if retinal scans were, for example, from the area centralis.

The primary risk factor[56] and only therapeutic target for glaucoma in dogs is an elevated IOP, yet disease progresses despite treatment in this multifactorial and incompletely understood disease. Findings in this series demonstrate that *in vivo* imaging of the retina and ONH in dogs can quantify structures relevant to glaucoma. With further validation of the technology for use in canine glaucoma patients, improved understanding of pathophysiological mechanisms, identification of early disease, and response to therapeutic interventions may become possible and improve treatment outcomes in dogs with this blinding and potentially painful disease.

Acknowledgements

The authors would like to thank the Canine Research Foundation for sponsorship that enabled the conduct of this study, and Optimed Pty Ltd, for provision of the Koeppe goniolens that was used in this study. We would also like to acknowledge those veterinarians and owners that assisted with recruitment for this study. Finally we wish to thank the anonymous reviewers whose input made a significant contribution to this manuscript.

References

1. Malik R, Swanson WH and Garway‐Heath DF. 'Structure‐function relationship' in glaucoma: Past thinking and current concepts. *Clinical and Experimental Ophthalmology*. 2012; 40(4): 369-380.

2. Sommer A, Katz J, Quigley HA*, et al.* Clinically detectable nerve fiber atrophy precedes the onset of glaucomatous field loss. *Archives of Ophthalmology*. 1991; 109(1): 77-83.

3. Wollstein G, Schuman JS, Price LL*, et al.* Optical coherence tomography longitudinal evaluation of retinal nerve fiber layer thickness in glaucoma. *Archives of Ophthalmology*. 2005; 123(4): 464-470.

4. Quigley HA, Katz J, Derick RJ*, et al.* An evaluation of optic disc and nerve fiber layer examinations in monitoring progression of early glaucoma damage. *Ophthalmology*. 1992; 99(1): 19-28.

5. Zeyen TG and Caprioli J. Progression of disc and field damage in early glaucoma. *Archives of Ophthalmology*. 1993; 111:62-62.

6. Chauhan BC, McCormick TA, Nicolela MT*, et al.* Optic disc and visual field changes in a prospective longitudinal study of patients with glaucoma: Comparison of scanning laser tomography with conventional perimetry

and optic disc photography. *Archives of Ophthalmology*. 2001; 119(10): 1492-1499.

7. Falsini B, Marangoni D, Salgarello T*, et al.* Structure–function relationship in ocular hypertension and glaucoma: Interindividual and interocular analysis by OCT and pattern ERG. *Graefe's Archive for Clinical and Experimental Ophthalmology*. 2008; 246(8): 1153-1162.

8. Chu F-I, Marín-Franch I, Ramezani K*, et al.* Associations between structure and function are different in healthy and glaucomatous eyes. *PloS One*. 2018; 13(5): e0196814. 10.1371/journal.pone.0196814

9. Miller WW and Parisi D. Development and validation of the canine visual function instrument. *Veterinary Ophthalmology*. 2018; 21(6): 586-594. 10.1111/vop.12551

10. Graham K, Byosiere SE, Feng L*, et al.* A forced‐choice preferential looking task for the assessment of vision in dogs: Pilot study. *Journal of Small Animal Practice*. 2018; doi.org/10.1111/jsap.12965doi.org/10.1111/jsap.12965

11. Annear MJ, Gornik KR, Venturi FL*, et al.* Reproducibility of an objective four‐choice canine vision testing technique that assesses vision at differing light intensities. *Veterinary Ophthalmology*. 2013; 16(5): 324-328.

12. Ezeh P, Myers L, Cummins K*, et al.* Utilizing an optokinetic device in assessing the functional visual acuity of the dog. *Progress in Veterinary Neurology*. 1990; 1(4): 427-432.

13. Garcia MM, Ying G-s, Cocores CA*, et al.* Evaluation of a behavioral method for objective vision testing and identification of achromatopsia in dogs. *American Journal of Veterinary Research*. 2010; 71(1): 97-102.

14. Odom J, Bromberg N and Dawson W. Canine visual acuity: Retinal and cortical field potentials evoked by pattern stimulation. *American Journal of Physiology-Regulatory, Integrative and Comparative Physiology*. 1983; 245(5): R637-R641.

15. Tanaka T, Ikeuchi E, Mitani S*, et al.* Studies on the visual acuity of dogs using shape discrimination learning. *Animal Science Journal*. 2000; 71(6): 614-620.

16. Willis CK, Quinn RP, McDonell WM*, et al.* Functional MRI as a tool to assess vision in dogs: The optimal anesthetic. *Veterinary Ophthalmology*. 2001; 4(4): 243-253.

17. Martins BC and Brooks DE. Diseases of the canine optic nerve. In: *Veterinary Ophthalmology* 5th edition (ed. KN Gelatt, BC Gilger and TJ Kern). John Wiley & Sons: Iowa. 2013; 1432-1474.

18. Brooks DE, Komaromy A and Kallberg M. Comparative optic nerve physiology: Implications for glaucoma, neuroprotection, and neuroregeneration. *Veterinary Ophthalmology*. 1999; 2(1): 13-25.

19. Spaeth GL. Development of glaucomatous changes of the optic nerve. In: *The optic nerve in glaucoma* (ed. R Varma, GL Spaeth and K Parker). JB Lippincott: Philadelphia. 1993; 63-81.

20. Smith SD, Singh K, Lin SC*, et al.* Evaluation of the anterior chamber angle in glaucoma. *Ophthalmology*. 2013; 120: 1985-1997.

21. Guedes V, Schuman JS, Hertzmark E, *et al.* Optical coherence tomography measurement of macular and nerve fiber layer thickness in normal and glaucomatous human eyes. *Ophthalmology*. 2003; 110(1): 177-189.

22. Leung CK-S, Cheung CYL, Weinreb RN, *et al.* Evaluation of retinal nerve fiber layer progression in glaucoma: A study on optical coherence tomography guided progression analysis. *Investigative Ophthalmology & Visual Science*. 2010; 51(1): 217-222.

23. Ittarat M, Itthipanichpong R, Manassakorn A*, et al.* Capability of ophthalmology residents to detect glaucoma using high-dynamic-range concept versus color optic disc photography. *Journal of Ophthalmology*. 2017; 2017:10.1155/2017/8209270

24. Tanito M. Optical coherence tomography observation of gonio structures during microhook ab interno trabeculotomy. *Journal of Ophthalmology*. 2017; 2017: 6310835-6310835. 10.1155/2017/6310835

25. Sato S, Ukegawa K, Nitta E, *et al.* Influence of disc size on the diagnostic accuracy of cirrus spectral-domain optical coherence tomography in glaucoma. *Journal of Ophthalmology*. 2018; 2018: 5692404. 10.1155/2018/5692404

26. Watanabe-Kitamura F, Inoue T, Kojima S, *et al.* Prospective 3D investigation of bleb wall after trabeculectomy using anterior-segment OCT. *Journal of Ophthalmology*. 2017; 2017: 8261364-8261364. 10.1155/2017/8261364

27. Bemis AM, Pirie CG, LoPinto AJ, *et al.* Reproducibility and repeatability of optical coherence tomography imaging of the optic nerve head in normal beagle eyes. *Veterinary Ophthalmology*. 2017; 20(6): 480-487.

28. Hernandez-Merino E, Kecova H, Jacobson SJ, *et al.* Spectral domain optical coherence tomography (SD-OCT) assessment of the healthy female canine retina and optic nerve. *Veterinary Ophthalmology*. 2011; 14(6): 400-405.

29. Grozdanic SD, Lazic T, Kecova H*, et al.* Optical coherence tomography and molecular analysis of sudden acquired retinal degeneration syndrome (SARDS) eyes suggests the immune‐mediated nature of retinal damage. *Veterinary Ophthalmology*. 2018, https://doi.org/10.1111/vop.125971-23. https://doi.org/10.1111/vop.12597

30. Young WM, Oh A, Williams JG*, et al.* Clinical therapeutic efficacy of mycophenolate mofetil in the treatment of SARDS in dogs–a prospective open‐label pilot study. *Veterinary Ophthalmology*. 2018; 21(6): 565-576.

31. Osinchuk SC, Leis ML, Salpeter EM*, et al.* Evaluation of retinal morphology of canine sudden acquired retinal degeneration syndrome using optical coherence tomography and fluorescein angiography. *Veterinary Ophthalmology*. 2018, doi.org/10.1111/vop.12602doi.org/10.1111/vop.12602

32. Beltran WA, Cideciyan AV, Guziewicz KE*, et al.* Canine retina has a primate fovea-like bouquet of cone photoreceptors which is affected by inherited macular degenerations. *PloS One*. 2014; 9(3): e90390. doi.org/10.1371/journal.pone.0090390

33. Iwabe S, Ying G-S, Aguirre GD*, et al.* Assessment of visual function and retinal structure following acute light exposure in the light sensitive T4R

rhodopsin mutant dog. *Experimental Eye Research*. 2016; 146: 341-353.

34. Beltran W, Acland G and Aguirre G. Morphologic analysis of retinal disease in the area centralis of RPGR-ORF15 mutant dogs. *Investigative Ophthalmology & Visual Science*. 2007; 48(13): 3718-3718.

35. Rodarte-Almeida ACV, Petersen-Jones S, Langohr IM, *et al.* Retinal dysplasia in american pit bull terriers‐phenotypic characterization and breeding study. *Veterinary Ophthalmology*. 2016; 19(1): 11-21.

36. Teixeira LB, Ver Hoeve JN, Mayer JA, *et al.* Modeling the chronic loss of optic nerve axons and the effects on the retinal nerve fiber layer structure in primary disorder of myelin. *Investigative Ophthalmology & Visual Science*. 2016; 57(11): 4859-4868.

37. Gekeler F, Gmeiner H, Völker M, *et al.* Assessment of the posterior segment of the cat eye by optical coherence tomography (OCT). *Veterinary Ophthalmology*. 2007; 10(3): 173-178.

38. Espinheira Gomes, F., Parry, S. and Ledbetter, E., *Spectral domain optical coherence tomography evaluation of the feline optic nerve and peripapillary retina.* Veterinary Ophthalmology, 2019. 10.1111/vop.12633(Epub ahead of print): p. 1-10.

39. Gonzalez-Alonso-Alegre EM, Rodriguez-Alvaro A and Esteban-Martín J. Atypical chorioretinal coloboma in a golden retriever: A retinographic, fluoroangiographic, and optical coherence tomography study. *Veterinary Ophthalmology*. 2016; 19(6): 525-530.

40. Gornik KR, Pirie CG, Duker JS*, et al.* Canine multifocal retinopathy caused by a BEST1 mutation in a boerboel. *Veterinary Ophthalmology*. 2014; 17(5): 368-372.

41. Hoffmann I, Guziewicz KE, Zangerl B*, et al.* Canine multifocal retinopathy in the australian shepherd: A case report. *Veterinary Ophthalmology*. 2012; 15: 134-138.

42. Schaefer EA, Whiting RE, Pearce JW*, et al.* Bilateral retinoschisis in a dog: A veterinary clinical application for optical coherence tomography. *Veterinary Ophthalmology*. 2018; 21(6): 668-674.

43. Grozdanic SD, Matic M, Betts DM*, et al.* Recovery of canine retina and optic nerve function after acute elevation of intraocular pressure: Implications for canine glaucoma treatment. *Veterinary Ophthalmology*. 2007; 10(s1): 101-107. 10.1111/j.1463-5224.2007.00584.

44. Shrout PE and Fleiss JL. Intraclass correlations: Uses in assessing rater reliability. *Psychological Bulletin*. 1979; 86(2): 420-428.

45. Lohr KN, Aaronson NK, Alonso J*, et al.* Evaluating quality-of-life and health status instruments: Development of scientific review criteria. *Clinical Therapeutics*. 1996; 18(5): 979-992.

46. McGreevy P, Grassi TD and Harman AM. A strong correlation exists between the distribution of retinal ganglion cells and nose length in the dog. *Brain, Behavior and Evolution*. 2004; 63(1): 13-22.

47. Peichl L. Topography of ganglion cells in the dog and wolf retina. *Journal of Comparative Neurology*. 1992; 324(4): 603-620.

48. Alamouti B and Funk J. Retinal thickness decreases with age: An OCT study. *British Journal of Ophthalmology*. 2003; 87(7): 899-901.

49. Poinoosawmy D, Fontana L, Wu J*, et al.* Variation of nerve fibre layer thickness measurements with age and ethnicity by scanning laser polarimetry. *British Journal of Ophthalmology*. 1997; 81(5): 350-354.

50. O'rese JK, Girkin CA, Budenz DL*, et al.* Effect of race, age, and axial length on optic nerve head parameters and retinal nerve fiber layer thickness measured by cirrus HD-OCT. *Archives of Ophthalmology*. 2012; 130(3): 312-318.

51. Zha, Y., Zhuang, J., Lin, D., et al., *Evaluation of myopia on retinal nerve fiber layer thickness measured by Spectralis optical coherence tomography.* Experimental and Therapeutic Medicine, 2017. **14**(3): p. 2716-2720.

52. Hood DC. Improving our understanding, and detection, of glaucomatous damage: An approach based upon optical coherence tomography (OCT). *Progress in Retinal and Eye Research*. 2017; 57: 46-75.

53. Wessel JM, Horn FK, Tornow RP*, et al.* Longitudinal analysis of progression in glaucoma using spectral-domain optical coherence tomography. *Investigative Ophthalmology & Visual Science*. 2013; 54(5): 3613-3620.

54. Sung KR, Sun JH, Na JH*, et al.* Progression detection capability of macular thickness in advanced glaucomatous eyes. *Ophthalmology*. 2012; 119(2): 308-313.

55. Na JH, Sung KR, Lee JR*, et al.* Detection of glaucomatous progression by spectral-domain optical coherence tomography. *Ophthalmology*. 2013; 120(7): 1388-1395.

56. Plummer CE, Regnier A and Gelatt KN. The canine glaucomas. In: *Veterinary Ophthalmology* 2nd edition (ed. KN Gelatt, BC Gilger and TJ Kern). John Wiley & Sons, Inc: Iowa. 2013; 1050-1145.

Figures and tables

Figure 1. (A) Optic nerve head located at the center of the scan (left eye) to allow comparison of measurements between subjects; B) schematic overlay demonstrating the sectors of the peripapillary retina that were analyzed for assessment of retinal thickness. Retinal thickness was assessed in quadrants (superior, nasal, inferior, temporal); eight sectors of the RNFL were assessed (*SN* superior, nasal; *ST* superior, temporal; *NU* nasal, upper; *NL* nasal, lower; *IN* inferior, nasal; *IT* inferior, temporal; *TU* temporal, upper; *TL* temporal, lower; *Sup* superior; *Nas* nasal; *Inf* inferior; *Temp* temporal).

Figure 2. Selection for appropriate scan quality and position. A) Retinal scan with a poor scan quality index showing distortion of the en face image to the left (dark regions at the top and bottom edges of the image), inadequate definition of retinal layers for manual segmentation, and the retina is not confined to the OCT window. Thickness map of case 1 showing appropriate positioning of the optic nerve head (B) taken after discarding the initial scan (C) due to excessive rotation of the globe shown with the dorsal retinal vein oriented to the temporal quadrant. Retinal crossline scan (scan orientation horizontal or vertical as indicated by the arrow in the top right corner) showing (D) inappropriate scan angle, and (E) repeat scan with appropriate positioning.

Figure 3. Schematic representation of where measurements for determining retinal thickness were obtained (highlighted yellow regions) when the circles are centered over the optic nerve head. The region of each quadrant that was within

the inner circle was excluded to minimize the impact of the optic nerve and intraocular myelin on measures of retinal thickness.

Figure 4. Retinal layer segmentation on B-scan image of the retina from case 1 (normal eye); A) retinal layers identified for manual segmentation of scans to measure retinal thickness including inner, outer and total retina, nerve fiber layer, ganglion cell complex. NFL = nerve fiber layer; GCL = ganglion cell complex layer; IPL = inner plexiform layer; INL = inner nuclear layer; OPL = outer plexiform layer; ONL = outer nuclear layer; ELM = external limiting membrane; PR = photoreceptors; RPE = retinal pigmented epithelium; B) definition of layers for measurement of retinal thickness: inner retina (from inner limiting membrane to inner plexiform layer), outer retina (from inner plexiform layer to retinal pigmented epithelium).

Figure 5. Three of the 20 B-scan images from case 2 showing manual adjustment of the lines demarcating the boundaries of the inner and outer retina (red arrows in [A]; the level at which retinal thickness is measured in each image is depicted in the en face image to the right). Where the optic nerve head and myelin were present, the lines were aligned to negate any measure of thickness in these regions (yellow arrows in [B-C]). D) Resulting thickness map showing the region of the ONH and intraocular myelin in black, reflecting the manual adjustments. S= superior; T= temporal; I= inferior; N= nasal. *The poorer image quality evident in Fig 4a-c is presented here as the only manner to show images of the modified individual B-scans was to take photographs of the computer screen as the analyses*

were being conducted. Position of temporal and nasal quadrants varies depending on whether the left or right eye is imaged.

Figure 6. Optic nerve head analysis. For manual identification of the outline of the ONH, 3D scans were assessed. Markers (on the right and below en face image) were maneuvered along the 6mm margins to show cross-sectional images of the retina in the horizontal and vertical planes at that level. Identification of the termination of the retinal pigmented epithelium and increased thickness associated with myelination could then be made prior to marking the ONH boundaries on the en face image (case 22).

Figure 7. B-scan image (left) and corresponding thickness map (right) demonstrating a thinner total retinal thickness in a predisposed left eye (case 17, bottom images) compared to a normal right eye (case 10, top images).

Figure 8. Scatterplot comparing measures of inner retinal thickness of the peripapillary retina in each quadrant showing a statistically significantly thinner inner retina in predisposed (diamonds) compared to normal eyes (circles).

Figure 9. Images of the optic nerve head and retinal nerve fiber layer obtained from normal (A. case 3, B. case 8) and predisposed eyes (C. case 15, D. case 19). The software which automatically detects the optic cup, failed to do so in some cases (e.g. A, C). The optic cup is represented in light grey in B and D.

Figure 10. Scatterplot comparing measures of peripapillary retinal nerve fiber layer (RNFL) thickness between normal (circles) and predisposed (diamonds) eyes in each quadrant.

Figure 11. Separate scans of the optic nerve head/retinal nerve fiber layer obtained to determine repeatability (consistency) of measurements (case 22, predisposed eye). Good consistency was seen when comparing the optic disc outline (dark grey) which required manual adjustments, but the consistency of automated measures such as the optic cup (light grey) which could not be manually adjusted was of limited applicability.

Figure 12. Assessment of intra-rater reliability determined by taking separate measurements (including manual adjustments) on the same optic nerve head/retinal nerve fiber layer scans with an interval of 6 months between analyses (case 6; normal eye). Excellent reliability was identified for measuring optic disc area (dark grey), while reliability of automated measures of optic cup (light grey) was adequate.

Table 1. Individual subject characteristics

Table 2. Characteristics of dog population studied

Table 3. Measures of retinal thickness in normal and predisposed eyes

Table 4. Retinal nerve fiber layer measurements

Table 5. Optic nerve head analyses

Table 6. Ganglion cell complex analyses

Table 7. Intra-class correlation coefficients for determination of repeatability (consistency) and intra-observer reliability

Table 1. Individual subject characteristics

I.D	Age yrs	Breed	Sex	Eye	Classification in study	Dx[a]	IOP[b] mmHg	Dilated IOP mmHg	Contralateral eye (IOP reported in mmHg)	Glaucoma duration (days)
1	6	Labrador X Poodle	MN	R	Normal	C	13	12	Normal*; IOP 12 (*15*)	N/A
2	9	Poodle	MN	L	Normal	C	12	10	Normal*; IOP 10 (*14*)	
3	6	Siberian Husky	FS	L	Normal	C	14	14	Entropion (excluded); IOP not measured	N/A
4	5	Pomeranian X	MN	R	Normal	C	13	13	Normal*; IOP 11	N/A
5	10	Jack Russell Terrier	FS	L	Normal	C	16	21	Previous trauma (cat scratch) (excluded); IOP 3	N/A
6	4	Cocker Spaniel	FS	R	Normal	C	10	14	Normal*; IOP 13 (*16*)	N/A
7	8	Shih Tzu	FS	L	Normal	C	8	10	Normal*; IOP 12 (*9*)	N/A
8	6	Labrador X Poodle	MN	R	Normal	C	12	12	Normal*; IOP 13 (*14*)	N/A
9	10	Australian Cattle Dog	MN	L	Normal	C	11	12	Traumatic cataract (excluded); IOP 3	N/A
10	9	Labrador X Poodle	FS	R	Normal	C	16	12	Normal*; IOP 15 (*12*)	N/A
11	10	Shih Tzu X	FS	L	Normal	C	13	19	Surgical pseudophakia (excluded); IOP 9	N/A
12	3	Terrier X	MN	L R	Normal	C	12 11	16 18	N/A. Mean measurement of both eyes used for analyses	N/A
13	9	Mansfield Terrier	FS	R	Predisposed[c]	C, U	15	17	Newly diagnosed primary glaucoma (latanoprost before/during imaging); IOP 40	36
14	12	Maltese X	M	R	Predisposed	C,U	8	14	Primary glaucoma (on topical latanoprost for months). IOP 64	90
15	10	Terrier X	FS	L	Predisposed	C,U	13	10	Primary glaucoma (on topical latanoprost for 2 weeks). IOP 48	14

16	9	Labrador X Poodle	FS	L	Predisposed	C,U	12	15	Primary glaucoma (on latanoprost and timolol /dorzolamide); IOP 62	65
17	12	Maltese	FS	L	Predisposed	C, U, H	13	22	Primary glaucoma (end stage at diagnosis; enucleated 4 months prior). Histology consistent with primary. Max IOP recorded 60	145
18	6	German Shepherd	FS	R	Predisposed	C, U, H	14	19	Primary glaucoma (end stage at diagnosis; enucleated). Histology consistent with primary. Max IOP recorded 56	350
19	6	Terrier X	MN	L	Predisposed	C,U	12	17	Primary glaucoma (end stage at diagnosis, IOP 67; evisceration and placement of ISP)	390
20	9	Labrador X Poodle	FS	L	Predisposed[c]	C,U	16	15	Newly diagnosed primary glaucoma (latanoprost before/during imaging); IOP 42 (maximum 72)	32
21	5	Terrier X	MN	R	Predisposed	C,U	15	20	Primary glaucoma (on latanoprost and timolol /dorzolamide); IOP 18 (82)	270
22	9	Maltese	FS	R	Predisposed	C,U	16	19	Primary glaucoma (on latanoprost and timolol /dorzolamide >12mths); IOP 6 (85)	420
23	10	Jack Russell Terrier	FS	R	Predisposed	C,U	14	17	Primary glaucoma (end stage at diagnosis, IOP 73; evisceration and placement of ISP)	75
24	6	Flat-Coated Retriever	FS	R	Predisposed	C,U, H	12	9	Primary glaucoma (end stage at diagnosis; enucleated). Histology consistent with primary. Max IOP recorded 56	450

[a]Dx = Method of diagnosis where C = clinical ophthalmic examination, U = ocular ultrasound, H = ocular histopathology following enucleation of globe; [b]as measured at time of imaging; [c]eye naïve to therapy at the time of imaging in a dog with glaucoma. *The mean measurements of this and the contralateral eye were used for analyses. Where a higher IOP was documented in that eye on a separate occasion, the highest documented measurement is recorded in parentheses. Post (tropicamide) dilation IOPs (when obtained) are underlined and italicised; MN = male neutered; FS = female spayed; L = left; R = right; IOP = intraocular pressure; N.R = no record; TSCP = transscleral cyclophotocoagulation;

Table 2. Characteristics of dog population studied

	Normal	Predisposed	*p* value*
Dogs	12	12	
Age (years)	7.2 (3-10)	8.6 (5-12)	0.231
Purebred dog	5/12 (41.7%)	6/12 (50%)	1.000
Sex (female)	6/12 (50%)	9/12 (75%)	0.400
IOP (mmHg)	12.5 (8-16)	13.5 (8-16)	0.366
Dilated IOP (mmHg)	12.5 (10-21)	17 (10-22)	**0.023**
Disease duration[a] (days)	N/A	194.8 (14-450)	N/A

Age, IOP and duration of glaucoma in subjects reported as median (range); IOP reported is that measured at the time of imaging; [a]disease duration is the time since diagnosis or reports of clinical signs consistent with glaucoma in the contralateral eye were recorded; **p* value reported for appropriate statistical comparisons between normal and predisposed dogs/eyes.

Table 3. Measures of retinal thickness in normal and predisposed eyes

		Normal	Predisposed	*p* value
Superior	**- Total**	204 (172-236)	199 (155-221)	0.154
	- Inner	107 (74-131)	85 (47-98)	**0.003**
	- Outer	101 (81-157)	116 (86-128)	**0.039**
Temporal	**- Total**	186 (152-223)	162 (105-188)	**0.005**
	- Inner	92 (70-114)	68 (37-89)	**0.001**
	- Outer	94 (79-131)	90 (57-116)	0.383
Inferior	**- Total**	178 (159 – 198)	158 (115-193)	**0.003**
	- Inner	86 (66-103)	65 (48-85)	**<0.001**
	- Outer	92 (80-119)	93 (67-118)	0.618
Nasal	**- Total**	179 (146-231)	164 (129-209)	0.191
	- Inner	91 (74-125)	78 (46-92)	**0.001**
	- Outer	90 (64-141)	88 (78-117)	0.639

Units for all measurements reported in μm; results expressed as median (range); *p* values <0.05 in bold

Table 4. Retinal nerve fibre layer measurements

	Normal	Predisposed	*p* value
TU	67.5 (48-144)	46 (30-91)	0.061
TL	83 (40-150)	51.5 (25-115)	**0.022**
Temporal	82 (48-206)	51.5 (28-102)	**0.034**
ST	96 (74-189)	78.5 (31-112)	**0.044**
SN	107 (86-150)	73.5 (21-123)	**0.002**
Superior	105 (82-148)	80 (26-104)	**<0.001**
NU	72.5 (51-130)	47 (19-81)	**0.007**
NL	107 (75-168)	68.5 (26-98)	**0.001**
Nasal	89.5 (69-149)	60.5 (22-84)	**0.001**
IN	80.5 (53-238)	61.5 (27-175)	0.111
IT	74 (49-173)	59.5 (27-121)	0.261
Inferior	79.5 (51-144)	64.5 (27-147)	0.234
Av thickn	92.5 (69-138)	62.5 (27-100)	**0.005**
Av sup	89.5 (72-134)	65.5 (26-87)	**0.003**
Av inf	90.5 (58-174)	63.5 (29-114)	**0.044**
Sup-inf	6 (-72 – 31)	-4.5 (-27 – 25)	0.734

Units for all measurements reported in μm; results expressed as median (range); *ST* superior-temporal, *SN* superior-nasal, *NU* nasal-upper, *NL* nasal-lower, *IN* inferior-nasal, *IT* inferior-temporal, *TL* temporal-lower, *TU* temporal-upper; *p* values <0.05 in bold

Table 5. Optic nerve head analyses

	Normal	Predisposed	*P* value
Cup: disc area	0.365 (0.05-0.54)	0.26 (0.08-0.84)	0.948
Cup: disc volume	0.66 (0.08-0.79)	0.5 (0.23-0.96)	0.983
Rim area	2.19 (1.08-5.37)	0.33 (4.5)	0.880
Disc area	3.59 (1.66-5.37)	3.01 (1.51-4.5)	0.597
Cup volume	0.11 (0.011-0.399)	0.026 (0.001-0.383)	0.174

Table 6. Ganglion cell complex analyses

	Normal	Predisposed	*P* value
Total GCC	85 (57-112)	70 (33-97)	0.164
Superior	83 (63-107)	78 (34-100)	0.354
Inferior	82 (50-118)	65 (32-95)	0.155
Intra-eye difference	8 (-11 – 21)	6 (-5 – 31)	0.705

Table 7. Intra-class correlation coefficients for determination of repeatability (consistency) and intra-observer reliability

Structure	Repeatability (n=11 eyes)	Intra-observer reliability (n=25)
Temporal retina		
- Total	0.773	0.824
- Inner	0.822	0.881
- Outer	0.794	0.909
Inferior retina		
- Total	0.748	0.942
- Inner	0.767	0.869
- Outer	0.753	0.843
Nasal retina		
- Total	0.787	0.902
- Inner	0.801	0.881
- Outer	0.815	0.893
Superior retina		
- Total	0.763	0.942
- Inner	0.797	0.878
- Outer	0.835	0.913
Retinal nerve fiber layer		
- Temporal, upper	0.781	0.742
- Temporal, lower	0.713	0.713
- Temporal, average	0.722	0.729
- Inferior, lateral	0.704	0.729
- Inferior, nasal	0.798	0.738
- Inferior, average	0.749	0.785
- Nasal, lower	0.735	0.727
- Nasal, upper	0.701	0.789
- Nasal, average	0.721	0.770
- Superior, nasal	0.713	0.737
- Superior, lateral	0.741	0.746
- Superior, average	0.720	0.741
- Average	0.742	0.756

- Average Dorsal	0.701	0.763
- Average Ventral	0.733	0.771
Ganglion cell complex		
- Total	0.600	N/A
- Dorsal	0.532	N/A
- Ventral	0.604	N/A
- Intra-eye difference	0.488	N/A
ONH		
- Cup: disc area	0.689	0.742
- Cup: disc volume	0.592	0.791
- Disc area	0.873	0.942
- Cup volume	0.598	N/A

vop_12694_f1.pdf

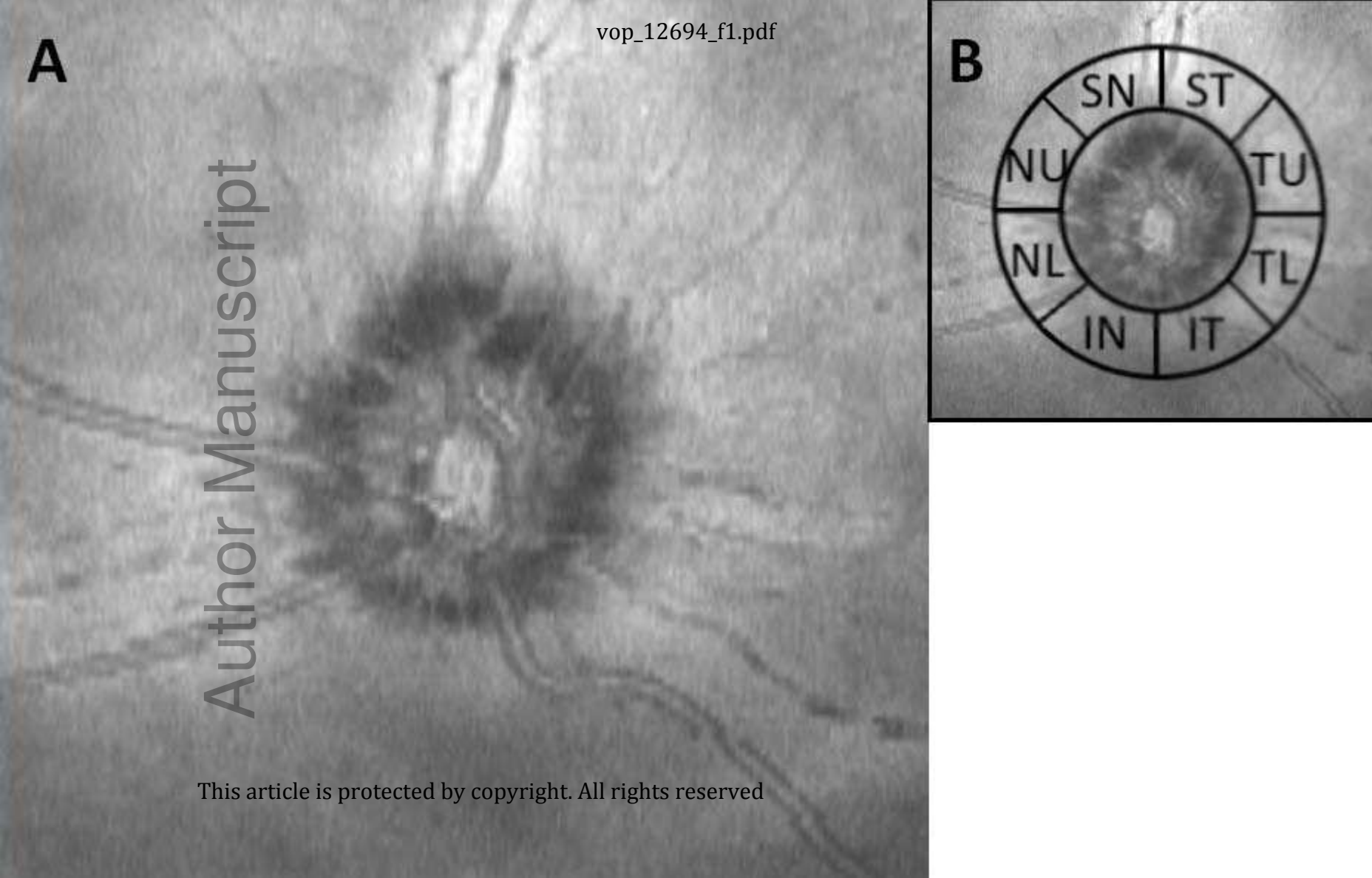


A.

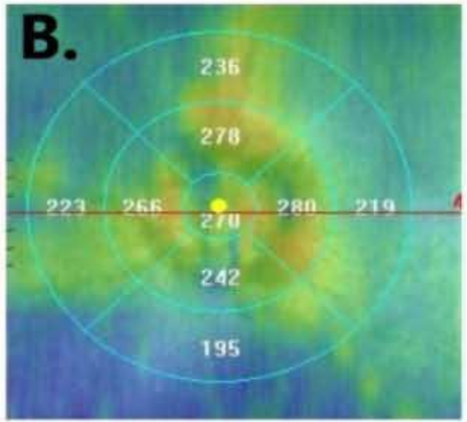
B.
236
278
223
266
270
280
219
242
195

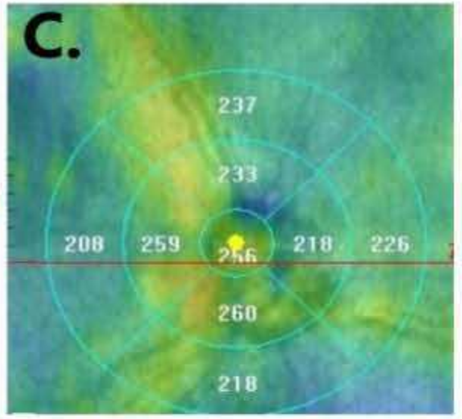
C.
237
233
208
259
256
218
226
260
218

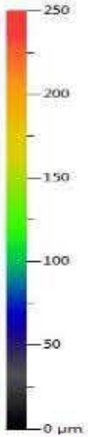
250
200
150
100
50
0 µm

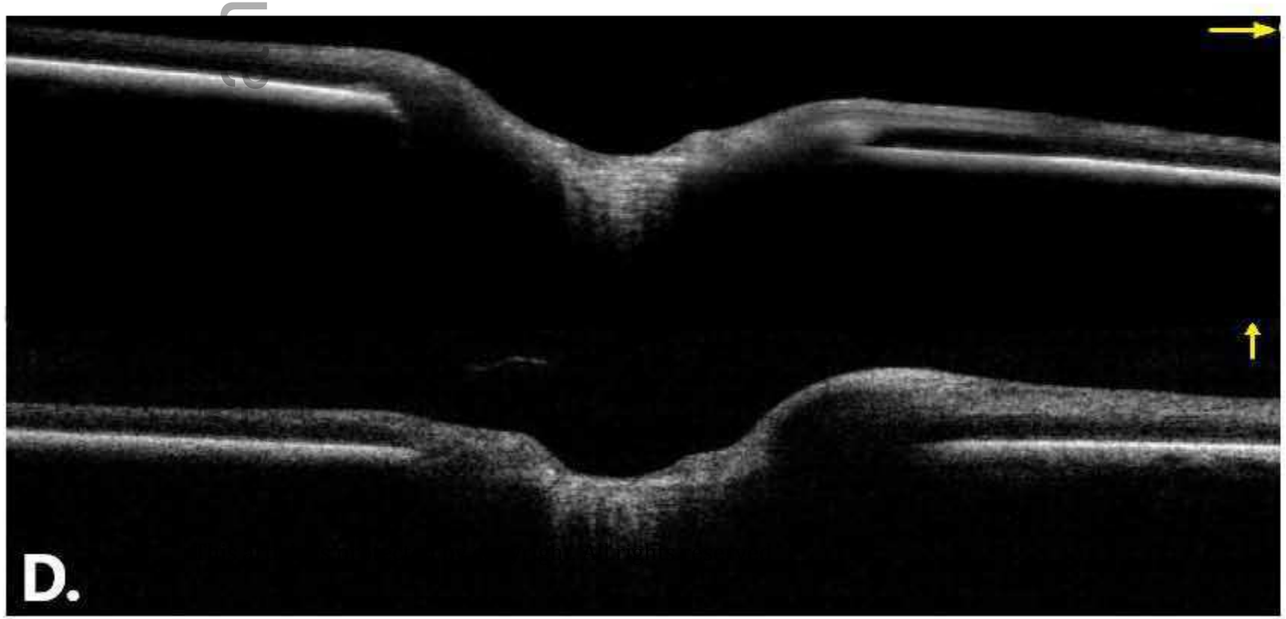
D.

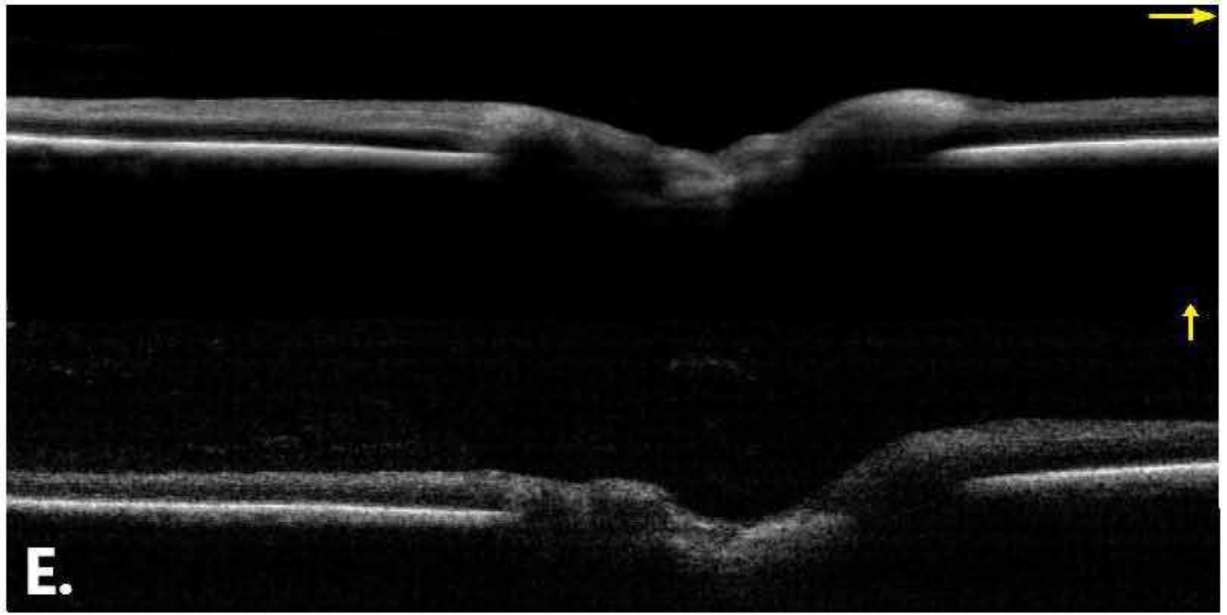
E.

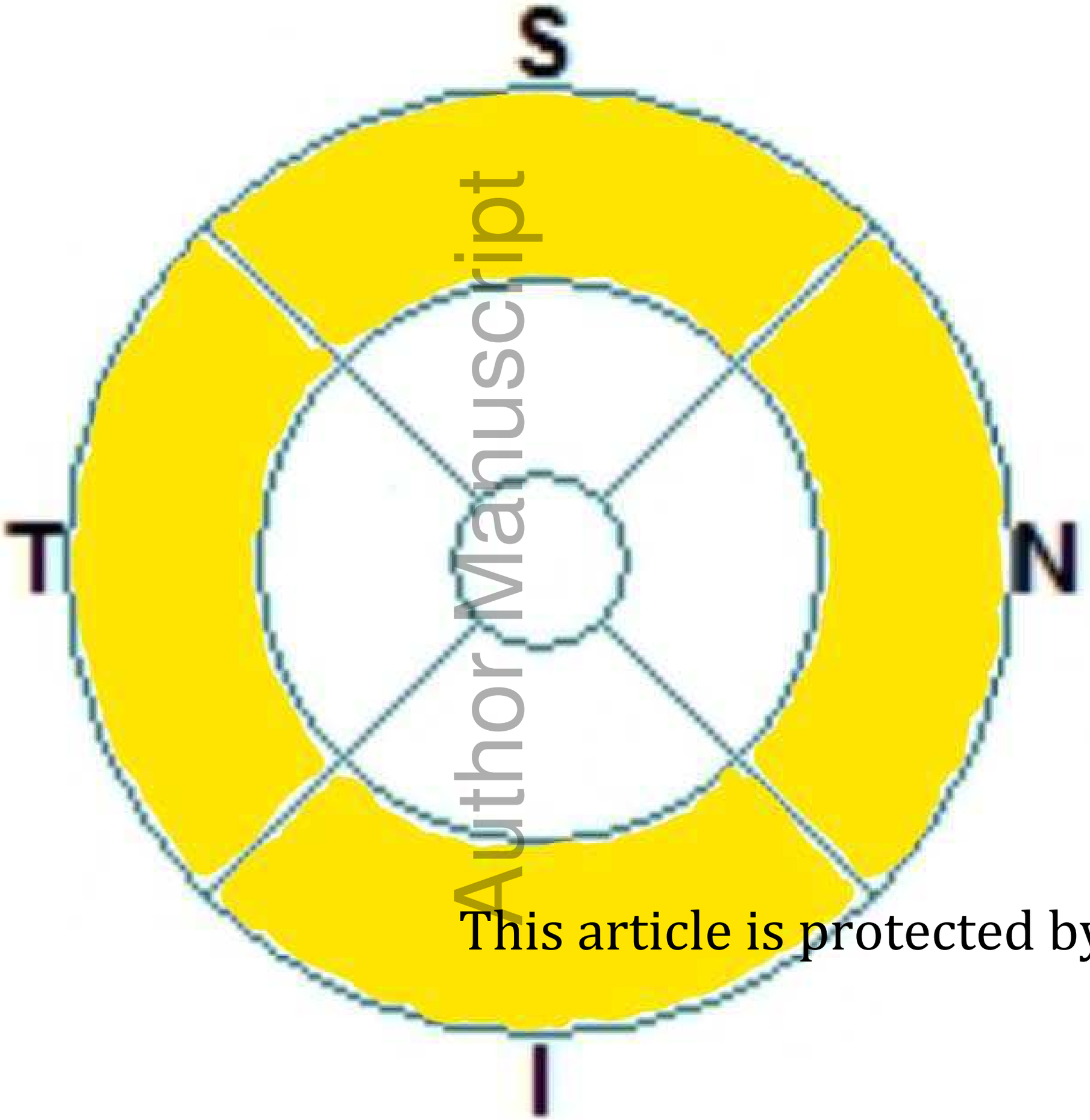

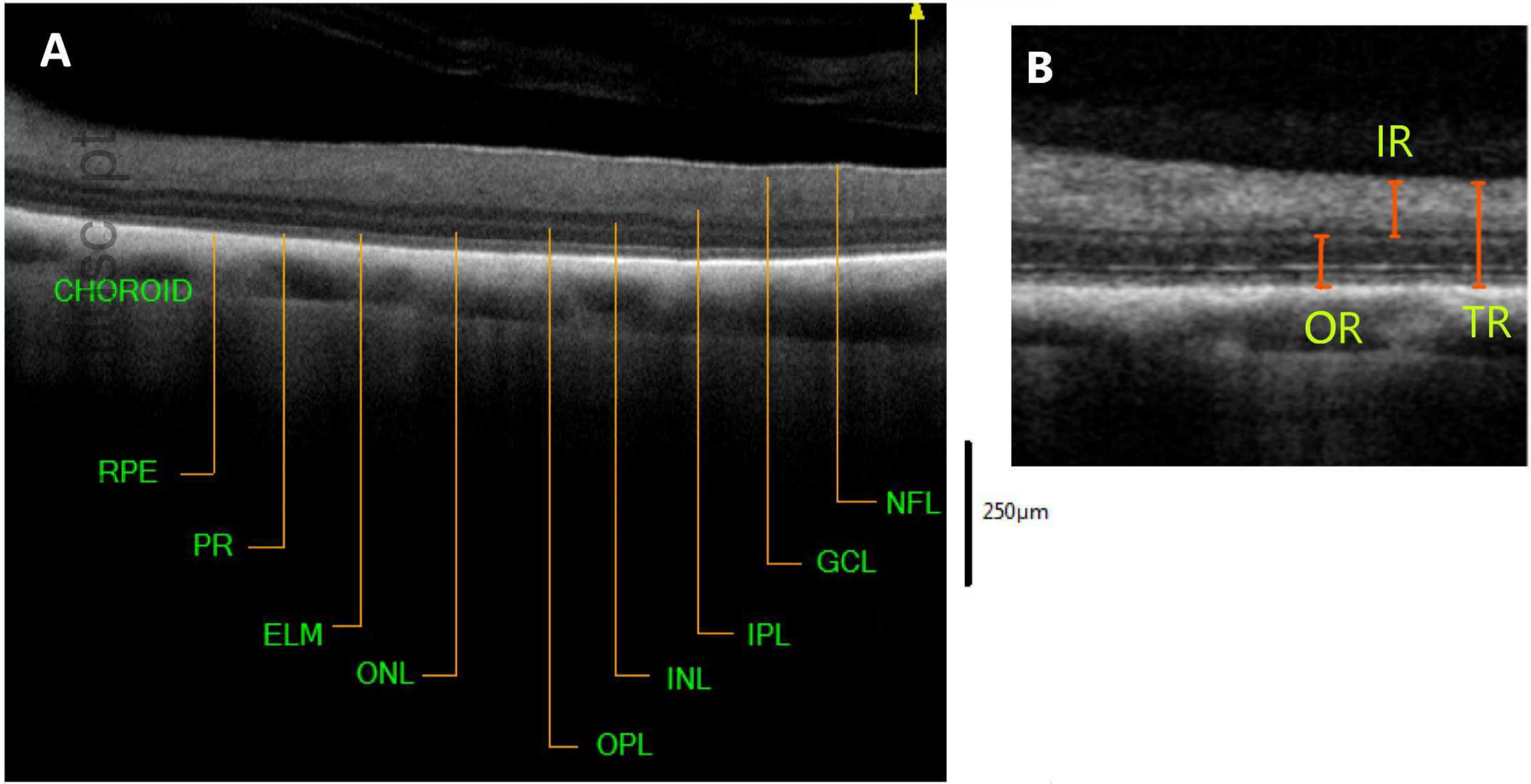
A
CHOROID
RPE
PR
ELM
ONL
OPL
INL
IPL
GCL
NFL
B
IR
OR
TR
250µm

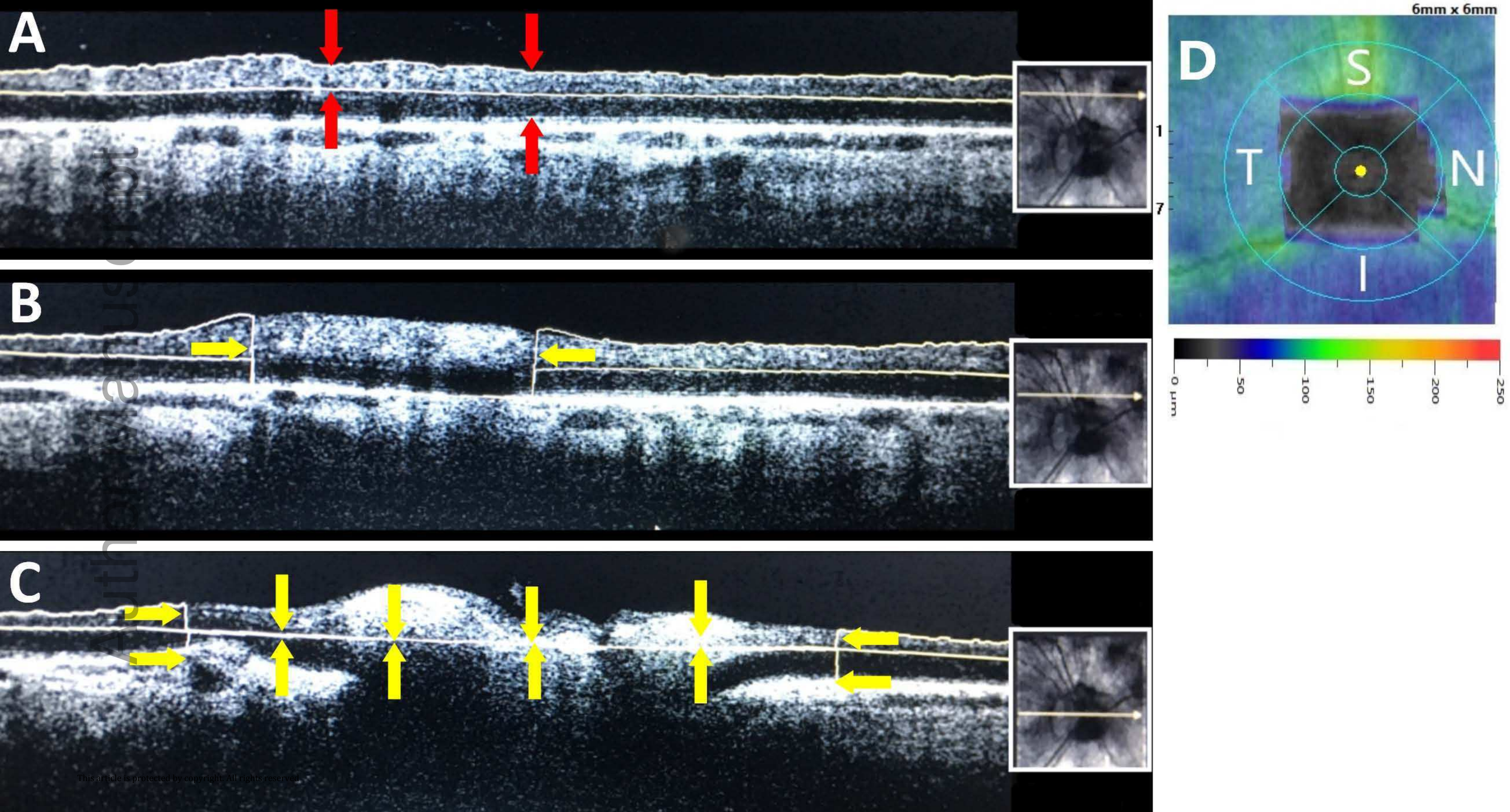

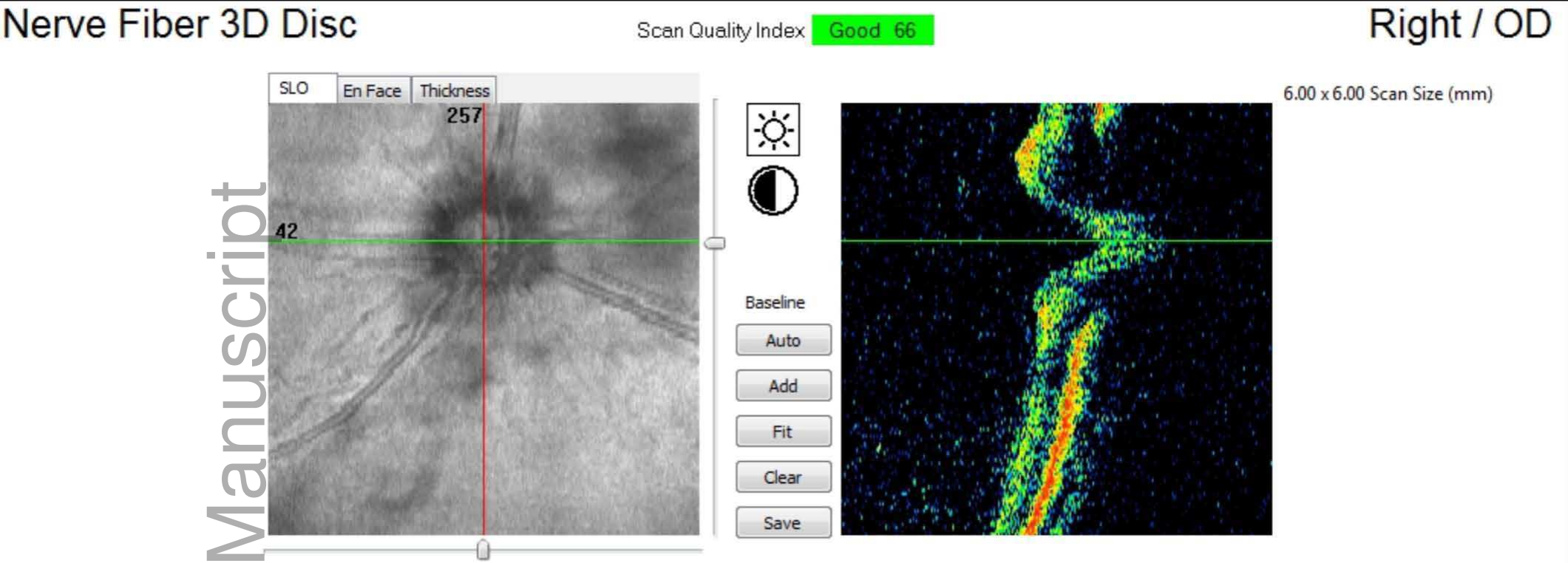

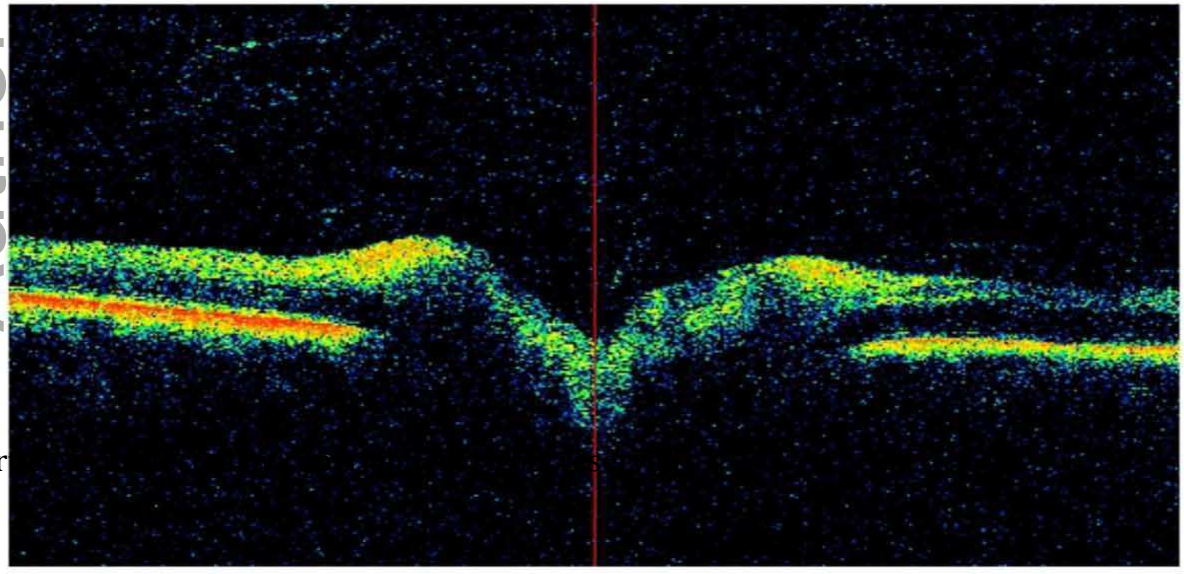

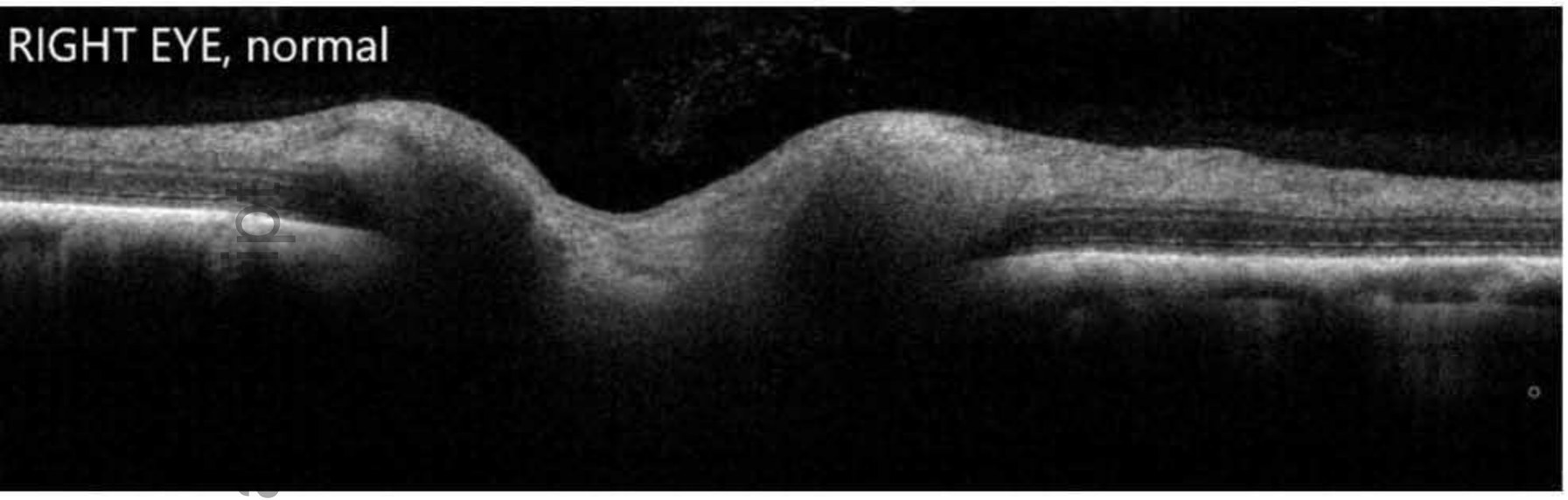
RIGHT EYE, normal

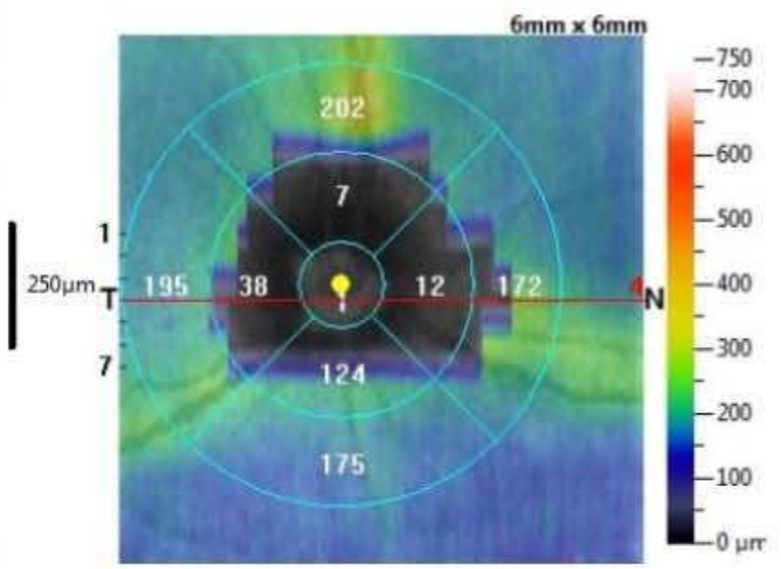
6mm x 6mm
202
7
195
38
12
172
124
175
T
N
1
7
250µm
750
700
600
500
400
300
200
100
0 µm

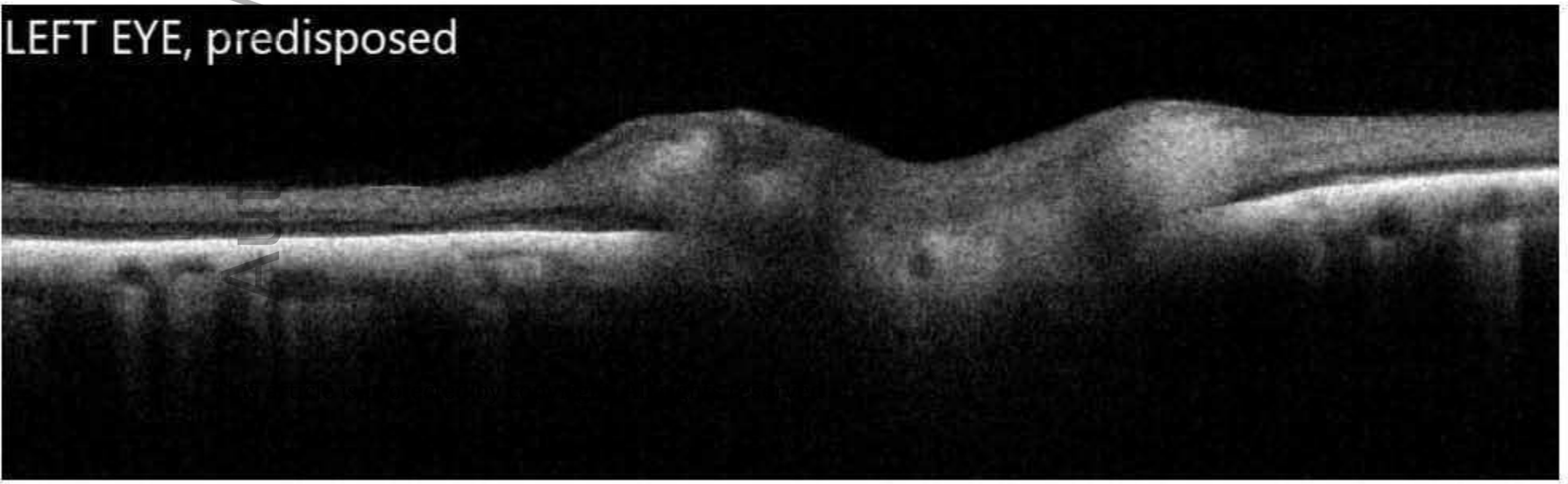
LEFT EYE, predisposed

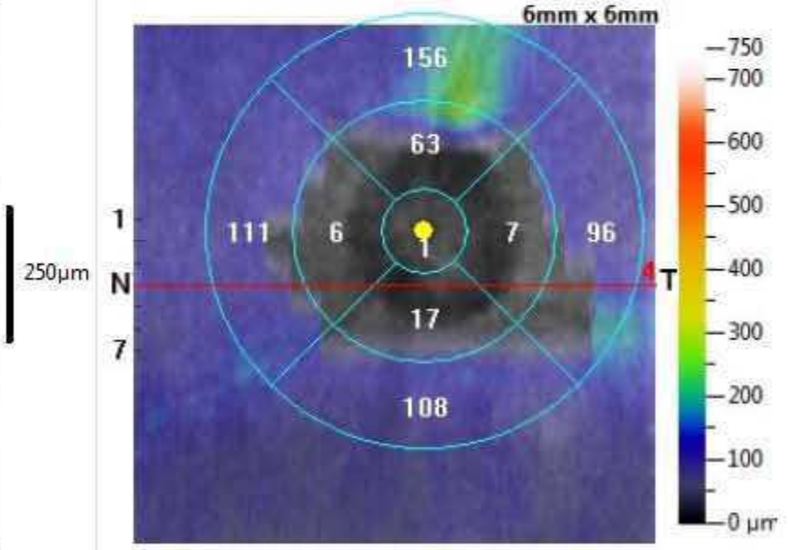
6mm x 6mm
156
63
111
6
7
96
17
108
N
T
1
7
250µm
750
700
600
500
400
300
200
100
0 µm

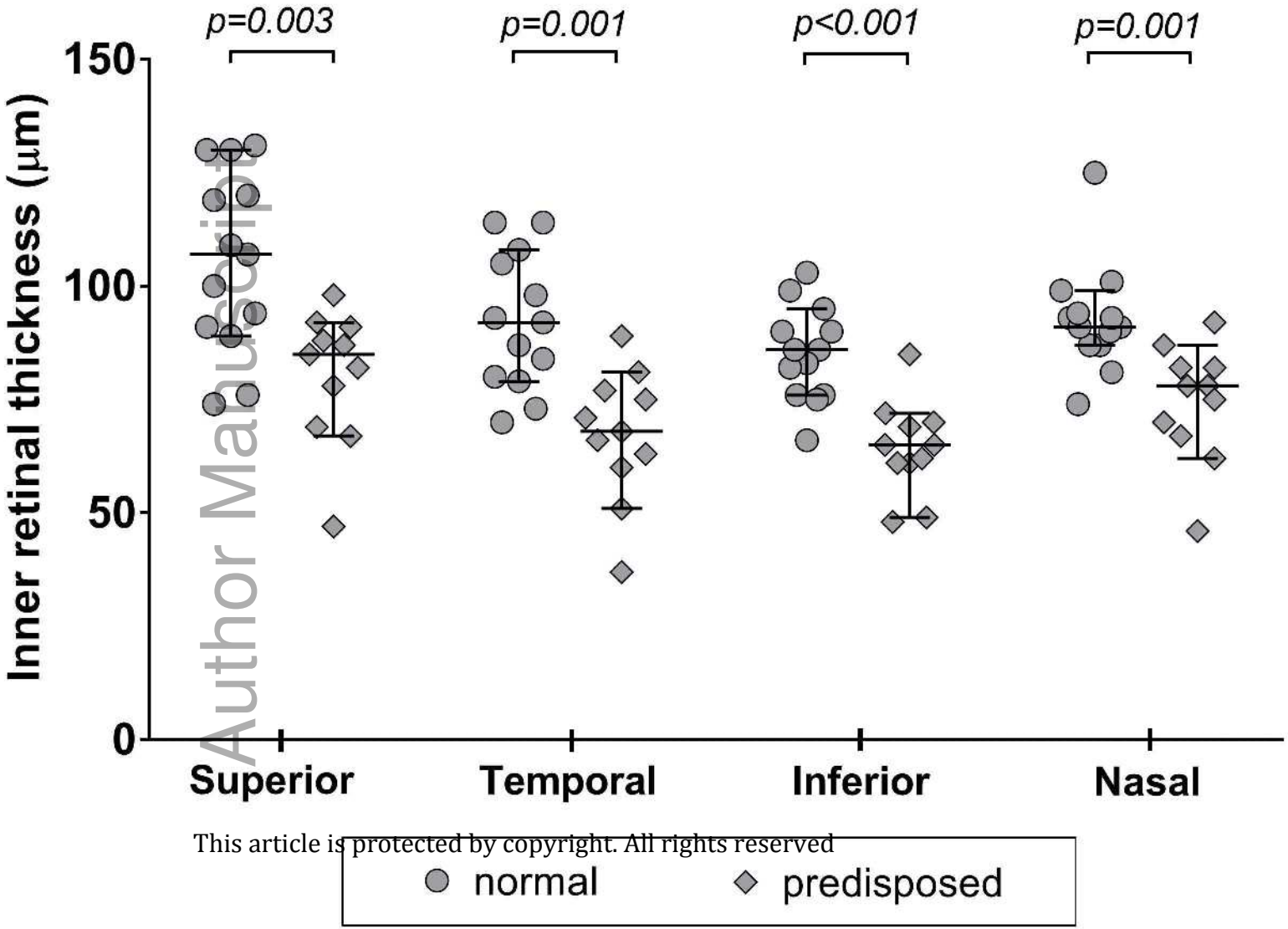

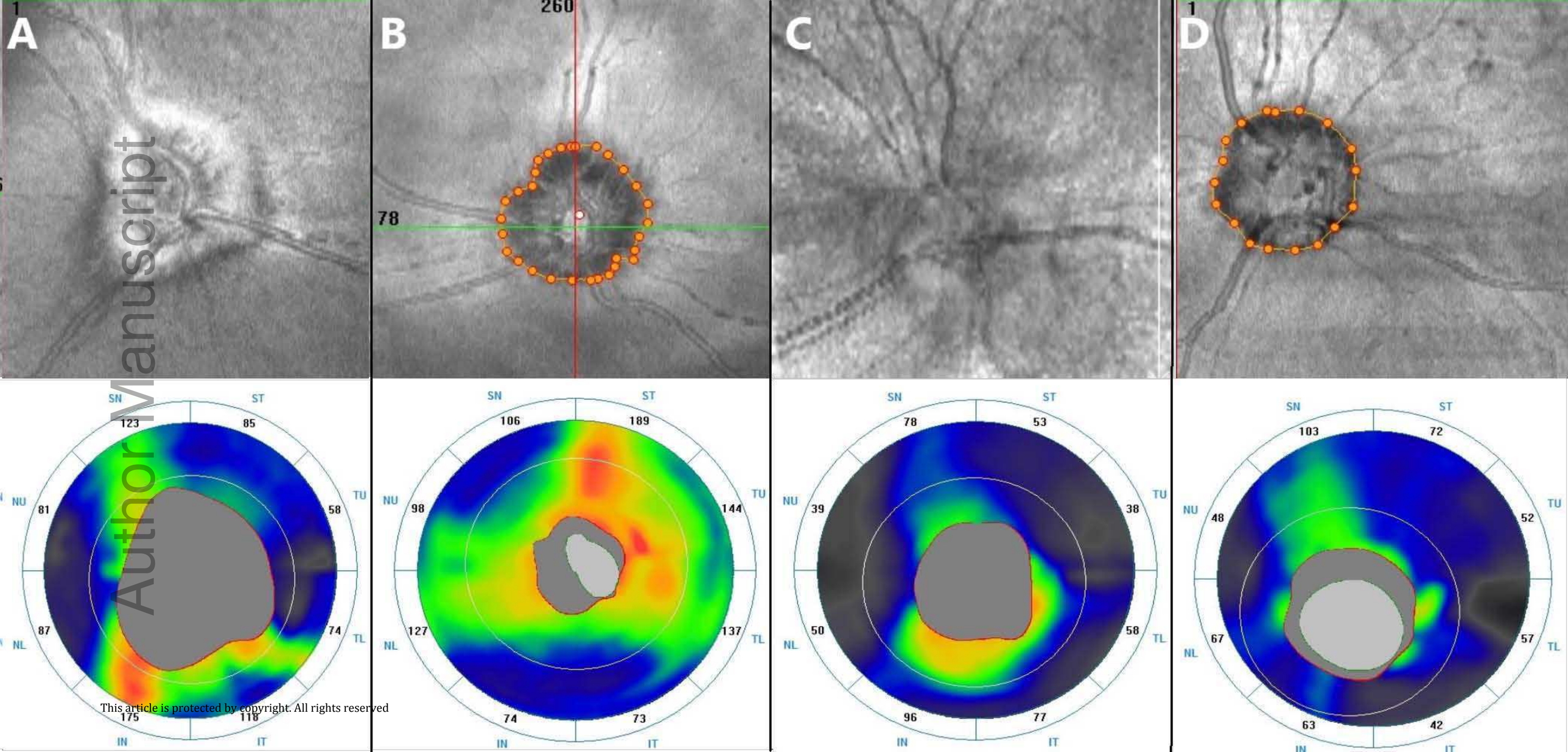

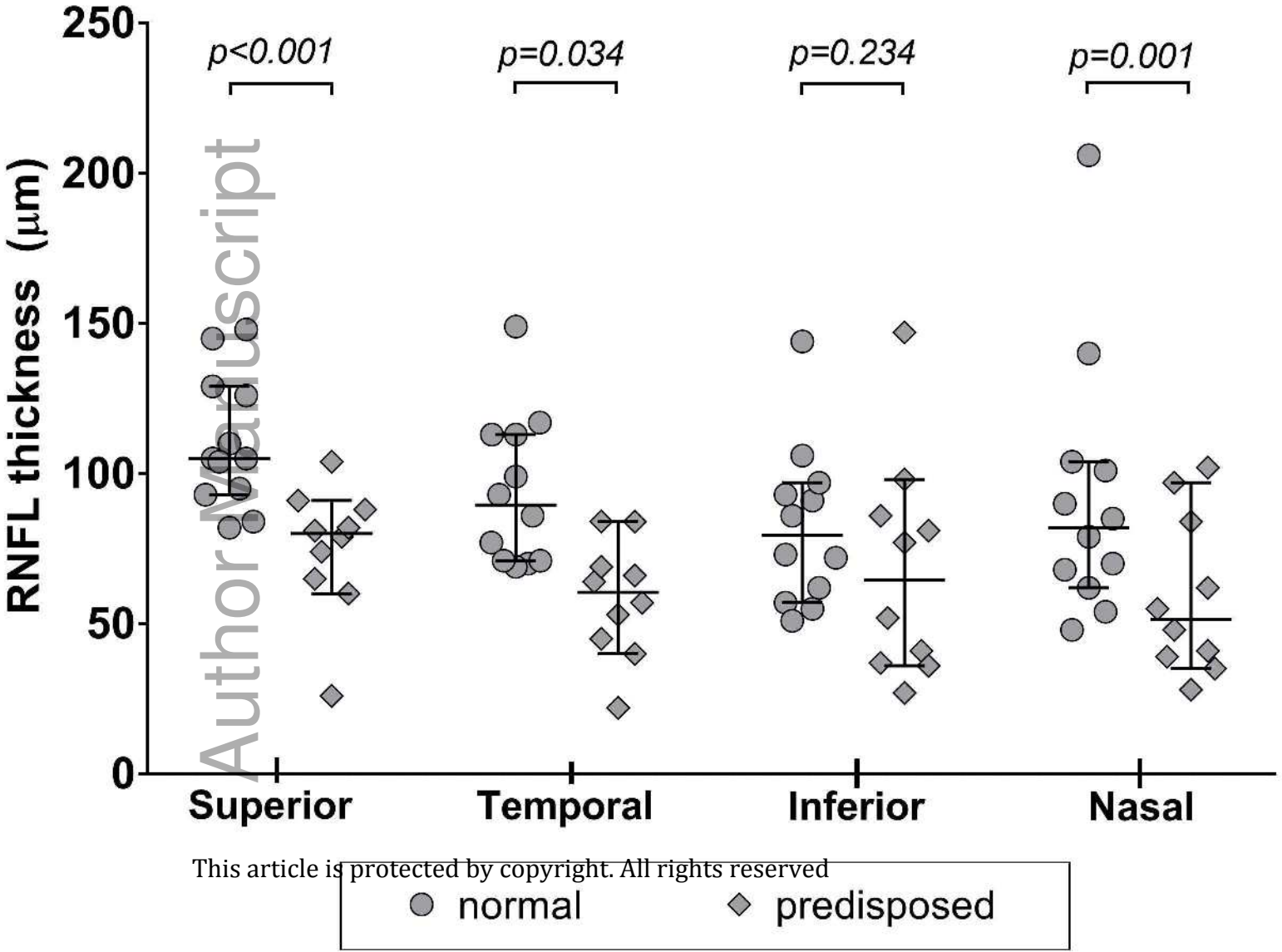

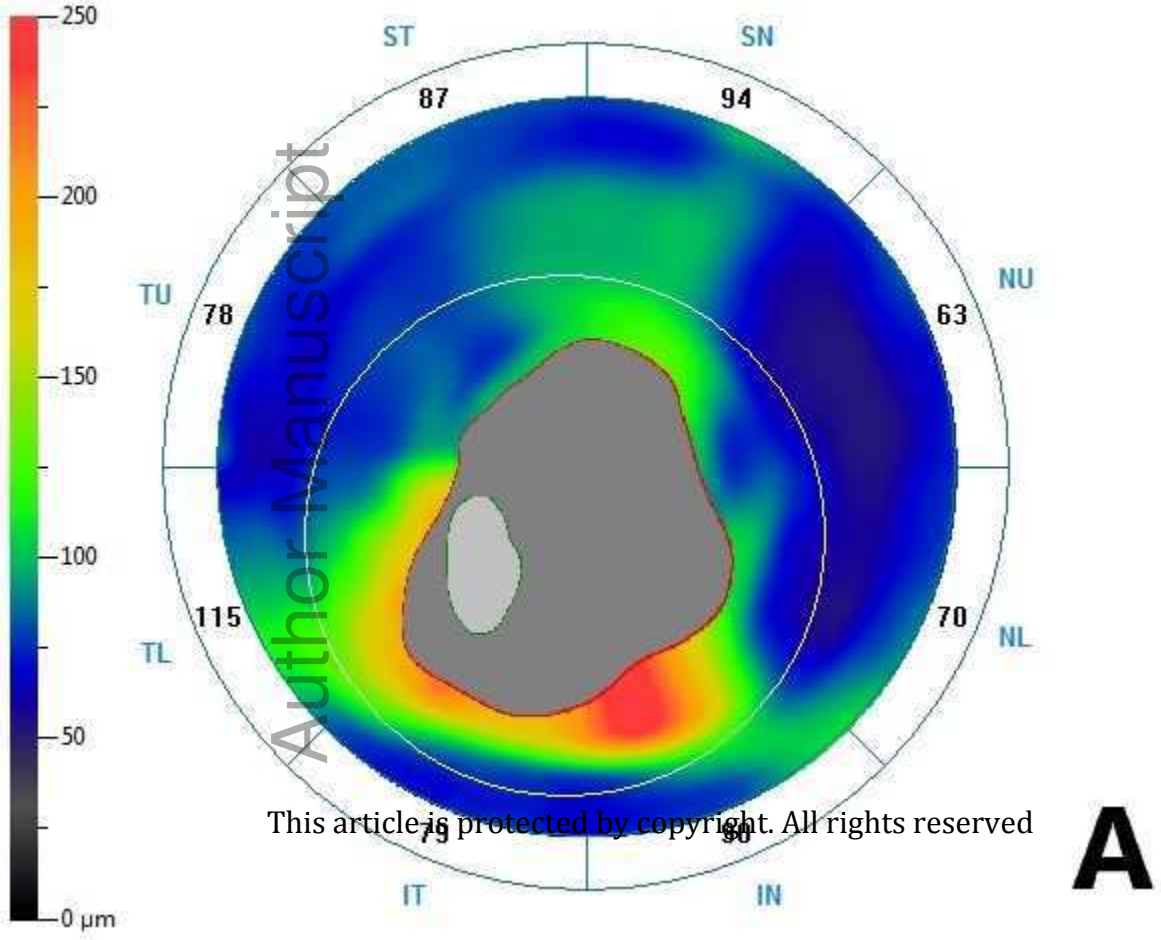

A

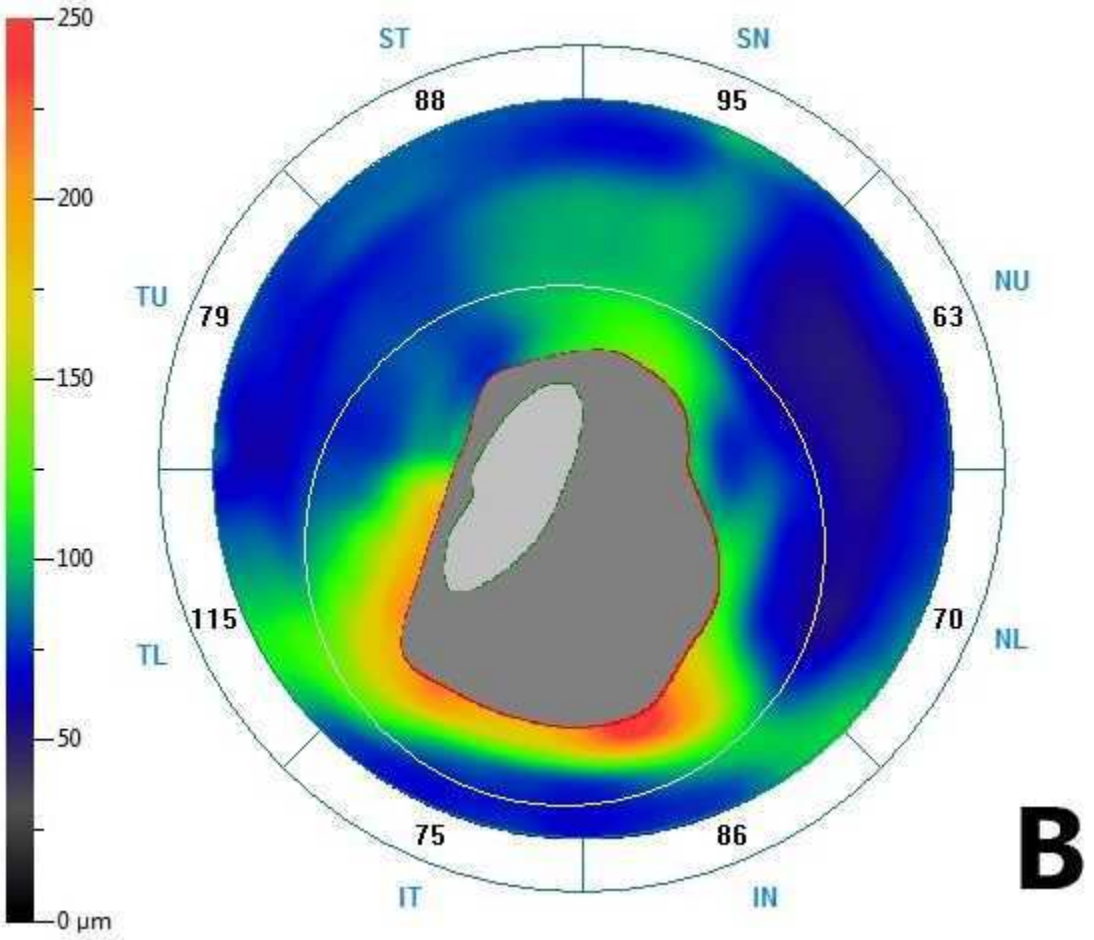

B